2020-06-24

DGAT1 is a lipid metabolism oncoprotein that enables cancer cells to accumulate fatty acid while avoiding lipotoxicity [preprint]

Daniel J. Wilcock
University of Manchester

Et al.

Let us know how access to this document benefits you.

Repository Citation

1 **DGAT1 is a lipid metabolism oncoprotein that enables cancer cells to**

2 **accumulate fatty acid while avoiding lipotoxicity**

3

4 Daniel J. Wilcock[1, *], Andrew P. Badrock[2, *, †], Rhys Owen[1], Melissa Guerin[3], Andrew D.

5 Southam[4, 5], Hannah Johnston[1], Samuel Ogden[2], Paul Fullwood[2], Joanne Watson[2],

6 Harriet Ferguson[2], Jennifer Ferguson[2], Daniel A. Richardson[1], Gavin R. Lloyd[4, 5], Andris

7 Jankevics[4, 5], Warwick B. Dunn[4, 5, 6], Claudia Wellbrock[1], Paul Lorigan[1, 7], Craig Ceol[3],

8 Chiara Francavilla[2, †], Michael P. Smith[2, §], and Adam F. L. Hurlstone[8, 9, §, &]

9

10 [1]Division of Cancer Studies, School of Medical Sciences, Faculty of Biology, Medicine and Health, The

11 University of Manchester, Manchester, M13 9PT, UK

12 [2]Division of Molecular & Cellular Function, School of Biological Sciences, Faculty of Biology, Medicine

13 and Health, The University of Manchester, Manchester, M13 9PT, UK

14 [3]Program in Molecular Medicine, Department of Molecular, Cell and Cancer Biology, University of

15 Massachusetts Medical School (UMMS), Worcester, MA 01605, Massachusetts, USA

16 [4]School of Biosciences, Edgbaston, University of Birmingham, Birmingham, B15 2TT, UK

17 [5]Phenome Centre Birmingham, University of Birmingham, Edgbaston, Birmingham, B15 2TT, UK

18 [6]Institute of Metabolism and Systems Research, University of Birmingham, Edgbaston, Birmingham, B15

19 2TT, UK

20 [7]and Department of Medical Oncology, The Christie NHS Foundation Trust, Wilmslow Road, Withington,

21 Manchester M20 4BX, UK

22 [8]Division of Infection Immunity and Respiratory Medicine, School of Biological Sciences, Faculty of

23 Biology, Medicine and Health, The University of Manchester, Manchester, M13 9PT, UK

24 [9]and Lydia Becker Institute of Immunology, The University of Manchester, Manchester, M13 9PT, UK

25

26 *These authors contributed equally

27 †Co-senior authors

28 §To whom correspondence should be addressed: Dr Michael P. Smith, Michael Smith Building, The

29 University of Manchester, Dover Street, Manchester M13 9PT, UK; tel: +44 161 2751586; email:

30 michael.smith-8@manchester.ac.uk: Orcid ID https://orcid.org/0000-0002-5980-7840. Dr Adam

31 Hurlstone, Michael Smith Building, The University of Manchester, Dover Street, Manchester M13 9PT,

32 UK; tel: +44 161 2751574; email: adam.hurlstone@manchester.ac.uk; Orcid ID https://orcid.org/0000-

33 0001-5260-9457; &Lead contact.

34

ABSTRACT

Dysregulated cellular metabolism is a hallmark of cancer. As yet, few druggable oncoproteins directly responsible for this hallmark have been identified. Increased fatty acid acquisition allows cancer cells to meet their membrane biogenesis, ATP, and signaling needs. Excess fatty acids suppress growth factor signaling and cause oxidative stress in non-transformed cells, but surprisingly not in cancer cells. Molecules underlying this cancer adaptation may provide new drug targets. Here, we identify Diacylglycerol O-acyltransferase 1 (DGAT1), an enzyme integral to triacylglyceride synthesis and lipid droplet formation, as a frequently up-regulated oncoprotein allowing cancer cells to tolerate excess fatty acids. DGAT1 over-expression alone induced melanoma in zebrafish melanocytes, and co-operated with oncogenic BRAF or NRAS for more rapid melanoma formation. Mechanistically, DGAT1 stimulated melanoma cell growth through sustaining mTOR kinase–S6 kinase signaling and suppressed cell death by tempering fatty acid oxidation, thereby preventing accumulation of reactive oxygen species including lipid peroxides.

SIGNIFICANCE

We show that DGAT1 is a *bona fide* oncoprotein capable of inducing melanoma formation and co-operating with other known drivers of melanoma. DGAT1 facilitates enhanced fatty acid acquisition by melanoma cells through suppressing lipototoxicity. DGAT1 is also critical for maintaining S6K activity required for melanoma cell growth.

2

58 **INTRODUCTION**

59 The continuous growth and survival of cancer cells is underpinned by dysregulated

60 cellular metabolism (1). Dysregulated cellular metabolism further promotes cancer

61 progression by reprogramming stromal cells, mediating evasion of immune responses,

62 and promoting metastasis (2-4). A central facet of cancer cell metabolism is a shift in

63 glucose usage away from oxidative phosphorylation towards biosynthetic reactions.

64 Without compensation by fatty acid oxidation (FAO) and glutaminolysis, this shift would

65 result in deficiencies in citric acid cycle intermediates needed for ATP production (1).

66 Although catabolism of fatty acids (FA) is needed to maintain ATP production,

67 increased lipogenesis (lipid generation) is simultaneously required for cell membrane

68 synthesis for which FA are principal building blocks (5). Furthermore, lipid signaling

69 molecules such as phosphatidyl inositides, diacylglycerides (DAG), lysophosphatidic

70 acid, and prostaglandins implicated in multiple cancer hallmarks (6) also require FA. To

71 satisfy these competing demands for FA, cancer cells increase its supply. This can be

72 achieved by initiation of *de novo* FA synthesis, normally a function of adipocytes and

73 hepatocytes, but an acquired characteristic of many cancer cells driven by elevated FA

74 synthase (FASN) expression (5). Alternatively, the additional FA needed can be

75 scavenged from the blood circulation as well as from abutting adipose tissue. Cancer

76 cells utilize secreted lipases such as lipoprotein lipase (LPL) to hydrolyze FA from

77 circulating triglycerides and FA transporter proteins (FATP) such as CD36 and the

78 SLC27 family of FATP and FA binding proteins (FABP) to facilitate uptake (7).

79 Enhanced uptake of extracellular FA by cancer cells has been established to promote

80 tumor growth and dissemination (8-10). Intracellular lipases can also be called on to

81 liberate FA from intracellular lipid stores, both through lipophagy or otherwise (11). One

82 such lipase, monoacylglycerol lipase (MAGL) is up-regulated in some aggressive

83 cancers, wherein its suppression impedes tumor growth and metastasis (12).

84   Regardless of the mechanism of acquisition, high levels of free FA come at a

85 cost to most cells. Non-adipose, untransformed cells that become overloaded with FA

86 display a constellation of effects termed lipotoxicity, characterized by reduced insulin

87 signaling (insulin resistance) and increased cell death (13). Multiple processes underlie

88 lipotoxicity, including increased ceramide synthesis, dysregulation of phospholipid

89 production that compromises mitochondrial and endoplasmic reticulum (ER) membrane

90 integrity, induction of reactive oxygen species (ROS), and impairment of ATP

91 generation (13). How, therefore, dysregulated metabolism favoring FA accumulation is

92 tolerated by cancer cells, and in particular how the toxic by-products of rampant FA

93 metabolism (principally reactive oxygen species [ROS] including lipid peroxides) are

94 suppressed or neutralized, is currently unclear. Targeting the ability of cancer cells to

95 manage potentially cytotoxic metabolites that arise from the rewiring of metabolic

96 pathways is an intriguing therapeutic avenue warranting further exploration (1).

97   *Bona fide* oncoproteins (defined as gene products whose up-regulation or coding

98 alteration contributes directly to neoplasia), for example BCR-ABL, BRAF^{V600E} or mutant

99 EGFR, are highly desirable molecular targets for precision treatment in cancers. Very

100 few druggable oncoproteins have been identified that are directly responsible for

101 dysregulating cellular metabolism. Among metabolic enzymes, only point mutations in

102 the isocitrate dehydrogenases IDH1 and IDH2 have been confirmed as oncogenic

103 drivers, but these mutations are detected in only 0.9%-3% of all cancers (14)

104 (Supplementary Figure 1A). While the gene encoding FASN is frequently amplified in

105   cancer (Supplementary Figure 1A), FASN inhibitors have so far failed to gain clinical

106   approval (15). Much of the metabolic reprogramming of cancer cells is achieved through

107   up-regulation of transcription factors including HIF1, MYC, peroxisome proliferator-

108   activated receptors (PPARs) and sterol regulatory element binding factors (SREBFs)

109   (16,17). However, these either lack druggable pockets or have diverse physiological

110   effects, detracting from their therapeutic potential. Thus, there is currently a dearth of

111   metabolism oncoproteins to pursue as therapeutic targets.

112   The small, fresh-water, tropical fish *Danio rerio*, commonly known as zebrafish,

113   has been embraced as a model for melanoma oncogene discovery and validation (18).

114   Previously, using zebrafish melanoma models, we identified a progression-associated

115   transcript signature enriched for lipid metabolism genes and we established enhanced

116   FA uptake as a characteristic of melanoma, driven in part by LPL (19). Here, we identify

117   frequent amplification and up-regulation of the gene encoding Diacylglycerol O-

118   acyltransferase 1 (*DGAT1*) in melanoma, among other cancers. DGAT1 is an ER-

119   resident enzyme that catalyzes the final step in triacylglyceride (TAG) synthesis from

120   diacylglyceride (DAG) and FA. DGAT1 is required for the formation of lipid droplets

121   (LD), cytosolic organelles comprising a core of neutral lipids (mainly triglycerides and

122   sterol esters) delimited by a monolayer of phospholipids, found in multiple cell types

123   (20). Furthermore, we demonstrate the ability of DGAT1 to induce melanoma formation

124   in zebrafish, and that DGAT1 exerts its oncogenic effect through shielding melanoma

125   cells from lipotoxicity, while enhancing cell growth through sustaining mTOR–S6K

126   signaling. As DGAT1 has been mooted as a clinical target for combating obesity,

127   several potent and selective small molecule inhibitors are already available for

128   repurposing (21) and we demonstrate their ability to suppress melanoma cell growth

129   and survival.

130

131   **RESULTS**

132   **Amplification and up-regulation of *DGAT1* associates with poor prognosis in**

133   **melanoma and multiple other cancers**

134   CD36, FATP1 and LPL that increase FA uptake into melanoma cells (9,19,22) are rarely

135   activated by point mutation, nor are the genes encoding them often amplified in cancer,

136   albeit that *CD36* amplification is enriched in established cancer cell lines

137   (Supplementary Figure 1A). Given the lack of metabolism oncoproteins to pursue as

138   therapeutic targets and the significance of lipid metabolism for melanoma development

139   (23), we further interrogated the lipid metabolism genes that we previously identified

140   accompany progression of mutant RAS driven melanoma in zebrafish (19). We plotted

141   their expression fold-change against association of expression of the human homologue

142   with patient survival. *dgat1a/DGAT1* emerged as an outlier, being both highly up-

143   regulated in zebrafish melanoma and significantly associated with reduced patient

144   survival (Figure 1A, B). In contrast, expression of the gene encoding the functionally

145   related, although structurally distinct, Dgat2/DGAT2 (20) did not change significantly nor

146   associate with patient survival (Figure 1A, B), indicating a possible unique function for

147   DGAT1 in melanoma. Furthermore, we confirmed elevated expression of human

148   *DGAT1* in melanoma tumors relative to both skin and nevi (Figure 1C) and elevated

149   DGAT1 protein in human melanoma cell lines relative to primary melanocytes

150   irrespective of NRAS or BRAF mutational status (Figure 1D).

6

151   We next considered what might underlie DGAT1 up-regulation in melanoma.

152   Visualization of structural alterations of the *DGAT1* gene in The Cancer Genome Atlas

153   firehose legacy cutaneous melanoma data set using cBioPortal revealed significant

154   focal amplification (as defined by the stringent GISTIC 2.0 algorithm) in up to 7 % of

155   melanoma cases with available copy number variation (CNV) data (but revealed no

156   microscale-aberrations). This frequency of focal amplification was comparable to that for

157   other recognized melanoma oncogenes (namely *CCND1*, *KIT*, *CDK4*, *MITF*, *TERT* and

158   *MDM2*; Figure 1E). An extra copy of the long-arm of chromosome 8 (8q), which

159   contains the *DGAT1* locus, but also other putative melanoma oncogenes *ASAP1*/*DDEF*,

160   *MYC* and *GDF6* (24-26) (Figure 1F), has been observed in approximately 30 % of

161   melanoma cases (27). Consistently, *DGAT1*, *ASAP1*, *MYC* and *GDF6* are co-amplified

162   in melanoma and other cancers (Supplementary Figure 1B, C), although there were

163   examples where each alone is amplified. However, of these four, high *DGAT1* mRNA

164   expression displayed the strongest association with reduced patient survival (Figure 1B

165   and Supplementary Figure 1D).

166   Further arguing for the significance of *DGAT1* amplification in melanoma

167   development, our previous comparative oncogenomic analysis (24) uncovered

168   amplification of *dgat1a* together with *gdf6b* (both on chromosome 19) in oncogenic-

169   BRAF driven zebrafish melanoma, concomitant with up-regulation of *dgat1a* and *gdf6b*

170   mRNA (Figure 1G and Supplementary Table 1). In contrast, neither *dgat1b* nor *gdf6a* on

171   chromosome 16, nor any *myc* or *asap1* paralogues (on chromosomes 2 and 24) were

172   amplified or up-regulated (Figure 1G, Supplementary Figure 1E, and Supplementary

173   Table 1).

174   Finally, we found *DGAT1* to be amplified in other human cancers arising from

175   distinct cell lineages, a feature of other well-characterized oncogenes, most notably in

176   up to 26% of cases of ovarian cancer (Supplementary Figure 1F). Strikingly, *DGAT1*

177   amplification was associated with significantly poorer progression-free survival across

178   multiple cancer types (Figure 1H). Thus, from a cancer genomics perspective, *DGAT1*

179   exhibits several hallmarks of an oncogene.

180

181   **Dgat1 functions as an oncoprotein in zebrafish melanocytes**

182   In human melanoma, *DGAT1* amplification was observed to co-occur with *BRAF* and

183   *NRAS* modification, but also independently of either (Figure 2A). To elucidate further the

184   oncogenic potential of *DGAT1*, we utilized a melanocyte rescue and lineage restricted

185   expression system as described previously (24,28). Remarkably, we found that Dgat1a

186   over-expression in zebrafish melanocytes lacking functional p53 was sufficient to induce

187   melanoma (Figure 2B), an outcome that we have only previously observed using the

188   potent well-established oncogenes RAS and BRAF. Moreover, Dgat1a over-expression

189   cooperated with both oncogenic BRAF and NRAS to accelerate the development of

190   nodular tumors (Figure 2C-E and Supplementary Figure 2A). Thus, in zebrafish, Dgat1

191   behaves as a melanoma oncoprotein. Significantly, Dgat2 over-expression was

192   indistinguishable from the non-oncogenic EGFP control (Figure 2D), indicating that

193   Dgat1-mediated tumorigenesis is specific and cannot be replicated by the functionally

194   related Dgat2.

195   To enable the development of hypotheses explaining how *DGAT1* is a potent

196   oncogene, we investigated the gene expression profile of melanoma tumors over-

197 expressing Dgat1a, utilizing RNA sequencing (RNA-seq). RNA-seq revealed an

198 average 5.5-fold increase in *dgat1a* mRNA expression compared to control EGFP-

199 expressing tumors (Figure 2F). Principal component analysis (Supplementary Figure

200 2B) and. hierarchical clustering (Supplementary Figure 2C) revealed patterns of gene

201 expression clearly distinguishing Dgat1a over-expressing tumors from EGFP-

202 expressing tumors. To pinpoint the biological processes providing context for selection

203 of DGAT1 up-regulation or that are potentially driven by DGAT1 up-regulation, we

204 compared the gene sets enriched in Dgat1a over-expressing tumors to those enriched

205 in the TCGA NRAS^{mut} DGAT1^{high} melanoma cohort compared to the rest of the NRAS^{mut}

206 tumor samples in the dataset (Figure 2G and Supplementary Figure 2E and

207 Supplementary Table 2). The overlap in enriched gene sets was only modest (Figure

208 2G) consistent with very few differentially expressed genes being shared in common

209 (Supplementary Figure 2F). However, this was not altogether unexpected given that the

210 genes whose expression most strongly correlated with *DGAT1* expression in human

211 tumors consistently mapped to chromosome 8q (data not shown) and were therefore

212 likely co-amplified with DGAT1, while *dgat1a* up-regulation in the zebrafish was driven

213 by randomly integrated transgene combined with expression of endogenous *dgat1a* on

214 a linkage group distinct from human 8q. Nonetheless, we hypothesized that the

215 conserved gene sets (Supplementary Table 2) would be the most relevant to

216 understanding the oncogenic role of *DGAT1*. Intriguingly, numerous of these conserved

217 gene sets indicated enhanced activation of mTOR signaling and protein translation, as

218 well as enhanced glycolysis and lipogenesis (Figure 2H), collectively indicative of

219 increased insulin sensitivity in tumors with up-regulated *dgat1a*/*DGAT1*. From this

9

220 analysis, therefore, we hypothesize that DGAT1 up-regulation modulates several

221 biochemical hallmarks of cancer which are conserved in both zebrafish and human

222 melanoma.

223

224 **DGAT1 enzymatic activity facilitates ribosomal protein S6-kinase (S6K)-**

225 **stimulated growth**

226 To ascertain which of the key oncogenic pathways highlighted by RNA-seq analysis of

227 tumors may be directly dependent on DGAT1, we examined the initial signaling

228 changes that occur when DGAT1 activity is suppressed, by performing unbiased

229 quantitative mass-spectrometry (MS)-based phospho-proteomics. We analysed

230 phosphorylated peptides from Stable Isotope Labelling in Cell Culture (SILAC)-labelled

231 DGAT1^{high} A375 melanoma cells following 4h treatment with A922500. This revealed

232 that DGAT1 activity affects cell growth and division signaling at mTOR, S6K and CDK1

233 signaling nodes (Figure 3A and Supplementary Figure 3A), mirroring the enrichment of

234 the mTOR and protein translation signatures revealed by gene set enrichment analysis

235 (Figure 2H). Western blotting to detect phosphorylated S6 and eEF2 confirmed that

236 DGAT1 inhibition led to rapid loss of mTOR and S6K activities in multiple melanoma cell

237 lines with up-regulated expression of endogenous DGAT1, including LOXIMVI and

238 SKMEL5 that harbor *DGAT1* amplification (Figure 3B and Supplementary Figure 3B).

239 This effect was not observed with DGAT2 inhibition (Supplementary Figure 3C).

240 Accordingly, DGAT1 depletion but not DGAT2 depletion using siRNA also resulted in a

241 reduction in phosphorylated S6 and accompanying increase in phosphorylated eEF2

242 (Figure 3C and Supplementary Figure 3D). Conversely, stable expression of DGAT1 in

10

243   DGAT1^{low} 888MEL melanoma cells (Figure 1D) as well as transient over-expression of

244   DGAT1 in two other melanoma cell lines resulted in elevated phospho-S6 (Figure 3D

245   and Supplementary Figure 3E).

246   Given the effect of DGAT1 antagonism on mTOR signaling, which is heavily

247   implicated in cell growth and division, we next addressed the importance of DGAT1 for

248   melanoma cell proliferation. DGAT1 depletion using siRNA reduced cell proliferation

249   and decreased the fractions of cells in S-phase (Figure 3C and Supplementary Figure

250   3G), which was in contrast to the increased proliferation and cell cycle progression

251   observed with stable DGAT1 overexpression (Figure 3D and Supplementary Figure 3F).

252   To determine whether these effects were due to the enzymatic function of DGAT1 we

253   utilized four selective DGAT1 inhibitors (AZD3988, AZD7687, A229500 or T863).

254   Pharmacological antagonism of DGAT1 suppressed melanoma cell growth over 96h

255   (Figure 4A), accompanied by decreased cell-cycle progression (Figure 4B).   In

256   contrast, no changes in cell growth or cell cycle progression were observed following

257   DGAT2 depletion or inhibition (Supplementary Figure 3B, C). Corroborating the link

258   between DGAT1, S6K activity, and proliferation, over-expression of wild-type p70S6K,

259   or a constitutively active form, partially restored cellular proliferation and phospho-S6

260   levels in DGAT1-suppressed melanoma cells (Figure 4C and Supplementary Figure

261   4D). Conversely, stable expression of DGAT1 in 888MEL melanoma enhanced cell

262   proliferation and this was reversed by pharmacological antagonism of S6K using

263   LY2584702 or PF-4708671 (Figure 4E). Taken together, we conclude that DGAT1

264   promotes melanoma cell proliferation by stimulating S6K activity.

265   Cancer cells are capable of sustaining cell growth despite transient or limited

266   nutrient availability in the tumor microenvironment arising from poor vascularization

267   (29). Given the connection suggested by gene set enrichment analysis between genes

268   differentially expressed in Dgat1a over-expressing tumors and HIF1 regulation of

269   glycolysis (Figure 2H), we investigated the role of DGAT1 in allowing cancer cells to

270   tolerate nutrient and oxygen deprivation in culture. First, we found that DGAT1

271   antagonism greatly impaired proliferation when external lipid sources were restricted,

272   with the greatest reduction in cell number observed at the lowest levels of serum (Figure

273   4F). The suppressive effect of DGAT1 inhibition on S6K activity was also observed in

274   lipid-restricted media (Supplementary Figure 4E). Second, we explored the importance

275   of DGAT1 under hypoxic conditions. Again, we found that DGAT1 inhibition had a

276   profound effect on cell number under low oxygen conditions, which was further

277   exacerbated by limiting serum (Figure 4G). Relative to growth of non-transfected cells,

278   transient DGAT1 overexpression augmented melanoma cell growth to a greater extent

279   under hypoxic conditions (Supplementary Figure 4F). Taken together up-regulation of

280   DGAT1 confers a growth advantage to melanoma cells, which is even more profound

281   under stress conditions likely to be encountered in the tumor microenvironment.

282

283   **DGAT1 is essential for lipid droplet formation and acts as a caretaker of**

284   **mitochondrial health**

285   The capacity of DGAT1 to sequester FA and DAG in LD has the potential to affect both

286   cell growth signaling and ATP production, as FA, DAG and their derivatives are

287   allosteric regulators of various metabolic enzymes, kinases and transcription factors,

288   and FA are also fuel molecules. Therefore, to address directly the effect of DGAT1 on

289   melanoma lipid metabolism using an unbiased approach, we performed Ultra-High-

290   Performance Liquid Chromatography-Mass-Spectrometry (UHPLC-MS) to identify and

291   contrast lipid species extracted from NRAS^{mut} Dgat1a over-expressing or NRAS^{mut}

292   EGFP-expressing zebrafish tumors. This analysis revealed increased concentrations of

293   almost all TAG species detected in tumors with forced Dgat1a expression, with longer

294   poly-unsaturated FA (PUFA) chains showing the greatest increases (Figure 5A,

295   Supplementary Figure 5A and Supplementary Table 3). However, after correction for

296   multiple testing, the changes were no longer significant. This lack of significance does

297   not necessarily disprove the hypothesis that DGAT can impact TAG levels, as several

298   experimental limitations exist that may confound the analysis. First, EGFP-expressing

299   tumors also over-express Dgat1a and have ample LD (19). Second, lipids originating

300   from associated stromal cells dilute the lipids derived from tumor cells. Both issues

301   mean that lipidome differences between Dgat1-over-expressing and EGFP-expressing

302   tumors are likely to be reduced in magnitude.

303   In order to overcome the complexity of whole tumor analysis, we turned to

304   melanoma cell lines. Over-expression of DGAT1 in human melanoma cells resulted in a

305   striking increase in LD (Figure 5B) consistent with cells adopting an engorged

306   morphology (Figure 5B). In parallel, UHPLC-MS lipidomic analysis revealed an increase

307   in almost all TAG species (Figure 5B and Supplementary Table 4, 5), corroborating the

308   trend in TAG seen in zebrafish tumors over-expressing Dgat1a (Figure 5A). Conversely,

309   inhibition of DGAT1 in melanoma cell lines over-expressing endogenous DGAT1 led to

310   a reduction in the amount of LD beginning between 12 and 24h and continuing until 72h

311 (Figure 5C and Supplementary Figure 5B, C), as previously reported for other cell types

312 (30). In contrast, LD were not affected by DGAT2 depletion (Supplementary Figure 5D).

313 As expected, UHPLC-MS lipidomic analysis revealed a reduction of multiple TAG

314 species already at 24h that was maintained until 72h, (Figure 5D, Supplementary Figure

315 5E and Supplementary Table 6, 7), with TAG containing PUFA particularly affected

316 (Supplementary Figure 5A).

317 Alongside the anticipated changes in TAG levels following manipulation of

318 DGAT1 activity, we also observed a decrease in several acyl carnitine (AcCa) species

319 upon DGAT1 overexpression (Figure 5B and Supplementary Table 4, 5) and a

320 reciprocal increase in AcCa species following DGAT1 inhibition (Figure 5D, E,

321 Supplementary Figure 5E and Supplementary Table 6, 7). AcCa, formed by

322 esterification of FA (typically long-chain) to L-carnitine, are transported into mitochondria

323 to be processed into acetyl-CoA through β-oxidation. The production of AcCa

324 determines the rate of FAO (31). PDK3 and PDK4 are mitochondrial kinases that

325 suppress conversion of pyruvate to acetyl-CoA when alternative fuel sources to

326 glucose, such as FA, are available (32). The increase in PDK3 and PDK4 activity we

327 detected following DGAT1 inhibition through our phospho-proteomic analysis (Figure

328 3A) was therefore consistent with increased AcCa availability and hence increased

329 FAO. Moreover, excessive FAO can result in mitochondrial overloading and dysfunction

330 (33). Indeed, we observed evidence of impaired ATP production following DGAT1

331 inhibition, implied by the increased phosphorylation of both AMPK and RAPTOR (Figure

332 5F). Further, we observed reduced oxygen consumption in DGAT1 inhibited cells after

333 48h (Figure 5G), implying decreased mitochondrial respiratory function despite levels of

14

334   AcCa remaining elevated (Figure 5D and Supplementary Figure 5E). Additionally, post

335   24h DGAT1 inhibition, we observed loss of mitochondrial membrane potential,

336   decreased PINK1 cleavage, and increased levels of mitophagy factor PARKIN (Figure

337   5H). Moreover, by blocking AcCa synthesis using Etomoxir (a carnitine

338   palmitoyltransferase inhibitor), we could partially restore mitochondrial membrane

339   potential and cell proliferation (Supplementary Figure 5F, G). Thus, we conclude that

340   DGAT1 maintains mitochondrial function in melanoma cells by regulating availability of

341   FA for FAO.

342

343   **DGAT1 promotes survival of melanoma cells in the presence of ROS**

344   To understand the effects of prolonged DGAT1 inhibition (post 72hr) on cellular

345   signaling and metabolism we performed unbiased MS-based whole proteome analysis

346   in SILAC-labelled A375 cells. Analysis of differentially expressed proteins highlighted

347   three key areas: i) FA oxidation (consistent with increased AcCa availability and PDK

348   activity), ii) PPAR signaling presumably indicating the increased availability of lipid

349   regulators of PPAR activity, and iii) NRF2 signaling, which is a well-established

350   response to ROS production that dampens ROS-mediated cellular damage (34) (Figure

351   6A, and Supplementary Figure 6A-B). Quantitative gene expression analysis further

352   corroborated the effects of DGAT1 inhibition on these three key biological processes

353   (Figure 6B and Supplementary Figure 6C).

354   To measure the impact of DGAT1 suppression on ROS more directly, we stained

355   cells with fluorescent probes that are uncaged by ROS. Using this method, we observed

356   increasing levels of ROS over time upon both DGAT1 inhibition and depletion in multiple

15

357 melanoma cell lines (Figure 6C,D and Supplementary Figure 6D,E), including in the

358 mitochondria specifically (Supplementary Figure 6F), a predicted consequence of

359 excessive FAO (33). Through a chain reaction, oxygen-centered ROS can yield highly

360 reactive cytotoxic lipid species termed lipid peroxides responsible for a form of

361 programmed cell death termed ferroptosis (35). Accordingly, in parallel with increased

362 ROS generation, DGAT1 inhibition led to an increase in the peroxidation of lipids from

363 24h, with further increases by 48h both in the cytoplasm (Figure 6E) and mitochondria

364 specifically (Figure 6F). Additionally, depletion of DGAT1 resulted in increased protein

365 attachment of 4-Hydroxynonenal (4HNE) (Figure 6G), a by-product of lipid peroxidation.

366 Conversely, we observed decreased protein attachment of 4-Hydroxynonenal (4HNE) in

367 DGAT1 over-expressing melanoma cells (Figure 6H) and also in zebrafish tumors over-

368 expressing Dgat1a (Figure 6I), indicating that lipid peroxidation and its suppression by

369 DGAT1 occurs not only in cell lines but also within tumors.

370   We next investigated whether the induction of ROS upon DGAT1 suppression

371 affected the survival of melanoma cells. In parallel with ROS generation, we observed

372 induction of ROS response markers, including SOD1 and SOD2 (Figure 7A,

373 Supplementary Figure 7A), and apoptosis induction in some DGAT1^{high} cell lines after

374 prolonged DGAT1 suppression (Figure 7A, B and Supplementary Figure 7B); again, an

375 effect not observed following DGAT2 inhibition (Supplementary Figure 7C, D).

376 Moreover, ROS scavengers Tempol and Ebselen partially suppressed apoptosis

377 induced by DGAT1 depletion (Figure 7B). Conversely, stable over-expression of DGAT1

378 in DGAT1^{low} 888MEL melanoma cells was protective against ROS-mediated cell death

379 triggered by chemical ROS inducers (Figure 7C). Further underpinning the observation

16

380   that DGAT1 confers a protective effect on melanoma cells in stressful conditions,

381   DGAT1 over-expression significantly increased cell survival under hypoxic conditions

382   (even with limited serum). Further, SOD2 induction was tempered by elevated DGAT1

383   activity, indicating suppression of ROS induction (Figure 7D). Thus, DGAT1 promotes

384   the survival of melanoma cells by suppressing ROS production and lipid peroxidation

385   that would otherwise occur as a result of cancer specific altered FA metabolism.

386   DGAT1 inhibition resulted in apoptosis only in a proportion of cells and in a

387   variable fraction dependent on cell line suggesting that not all affected cells produce

388   toxic ROS levels. We therefore hypothesized that anti-ROS mechanisms were activated

389   in some cells, counteracting the effects of DGAT1 suppression. We wanted to

390   investigate how the anti-ROS response was being coordinated downstream of DGAT1

391   inhibition in order to identify targets that might synergize with DGAT1 inhibition. mRNA

392   for the NRF2 target *SESTRIN2 (SESN2)* was found to be highly up-regulated post

393   DGAT1 inhibition (Figure 6B). Accordingly, SESN2 protein was consistently and

394   significantly up-regulated in a panel of melanoma cell lines following DGAT1 inhibition

395   (Figure 7E). Intriguingly, SESN2 is a major mediator of NRF2 signaling responsible for

396   neutralizing ROS while simultaneously inhibiting mTOR signaling (36). This suggests

397   that SESN2 induction may mediate, but also ameliorate the impact of DGAT1 inhibition

398   on cell growth and survival. Supporting this hypothesis, simultaneous depletion of

399   SESN2 and DGAT1 resulted in a greater reduction in surviving cell numbers (Figure

400   7F), coinciding with increased apoptosis, compared to DGAT1 depletion or inhibition

401   alone (Figure 7F, Supplementary Figure 7E). Simultaneous knockdown of SESN2 and

402   inhibition of DGAT1 (Supplementary Figure 7F) also led to both elevated levels of ROS

17

403   (Figure 7G) and increased expression of the NRF2 target gene HMOX1 (Figure 7H)

404   compared to DGAT1 inhibition alone, indicating that without SESN2 induction the

405   neutralization of ROS is impaired. Moreover, we found that the reduction of mTOR

406   signaling induced by DGAT1 inhibition was alleviated by knockdown of SESN2

407   (Supplementary Figure 7G). Thus, SESN2 acts as a counterfoil to DGAT1, suppressing

408   mTOR signaling while ameliorating ROS inflicted damage.

409

410   **DISCUSSION**

411   The role of dysregulated lipid metabolism, encompassing more than just *de novo* FA

412   synthesis, in promoting neoplasia is increasingly apparent (8,9,12,37). However, the

413   adaptations allowing cancer cells to tolerate exposure to excess FA have been

414   overlooked. Using multiple zebrafish models, integrating outputs across multiple omics

415   platforms, including oncogenomic, transcriptomic, proteomic, phospho-proteomic, and

416   lipidomic, combined with assays of cell behavior, we now demonstrate that DGAT1 is a

417   novel *bona fide* metabolism oncoprotein that stimulates melanoma tumorigenesis. We

418   conclude that DGAT1 promotes proliferation through mTOR–S6K signaling. We also

419   show that DGAT1 promotes survival principally by conferring protection against ROS

420   and lipid peroxidation through inducing LD formation (see model; Supplementary Figure

421   7H).

422   We uncovered frequent amplification and up-regulation of *DGAT1* in melanoma

423   but also in many other cancers, notably ovarian, breast, uterine, esophageal, liver,

424   pancreatic, head and neck, prostate, stomach and lung cancers. Abundant LD have

425   been observed in a range of cancers, consistent with widespread up-regulation of

18

426   DGAT1 (38,39), indicating that DGAT1 is likely to perform an oncogenic role in these

427   other cancers too. The co-occurrence of *DGAT1* amplification with *FASN*, *CD36*, or

428   *MAGL* amplification in human cancers was significant (data not shown), arguing for

429   these co-aberrations being synergistic, in keeping with DGAT1 facilitating safe

430   accumulation of FA in cancer cells.

431   Multiple indirect mechanisms connect DGAT1 enzymatic activity with S6K

432   activity. On the one hand, by promoting mitochondrial respiratory function and ATP

433   generation, DGAT1 suppresses AMPK thereby relieving inhibition of mTOR (40).

434   Further, through curbing ROS generation by malfunctioning mitochondria, DGAT1

435   activity represses NRF2 activation and induction of SESN2, a known inhibitor of mTOR

436   (36). Accordingly, knockdown of SESN2 rescued the S6K suppression ensuing DGAT1

437   inhibition. Other potential DGAT1-dependent factors that could impact mTOR signaling

438   include phosphatidic acid, essential for mTOR activity (41), and DAG, which co-activate

439   PKC that in turn inhibit growth factor signaling to mTOR (42). Levels of these lipids

440   could be rapidly affected by DGAT1-driven sequestration of DAG and FA as TAG in LD.

441   However, changes in concentration of these lipid species following manipulation of

442   DGAT1 activity or expression were not readily apparent from our lipidomics analyses,

443   perhaps limited by their low abundance, instability, rapid association with proteins in the

444   cell, or a combination of all the above. Intriguingly, mTOR–S6K signaling has been

445   shown to induce lipogenesis and LD formation (37,43,44), suggesting that mTOR

446   signaling and lipogenesis are mutually re-enforcing events.

447   We propose that sequestration of FA as TAG in LD allows cancer cells to

448   accumulate and utilize FA safely, thereby avoiding cell death. As previously described in

19

449 non-transformed embryonic fibroblasts (30), we observed that DGAT1 suppression

450 resulted in overloading of mitochondria with AcCa, driving excessive FAO and ROS

451 production. Thus, the pathophysiological role of DGAT1 is to regulate the supply of FA

452 to mitochondria within safe limits. Evidently, cancer cells, having elevated FA, require

453 more DGAT1 to achieve this. Lipid peroxides are especially cytotoxic and are generated

454 by the action of oxygen-centered radicals on polyunsaturated fatty acids (PUFA)

455 preferentially (45). As PUFA are concentrated in LD where they are shielded from

456 peroxidation (46), enhanced LD levels mediated by DGAT1 up-regulation confer double

457 protection from cell death by both moderating FAO-triggered ROS production and

458 simultaneously shielding them from PUFA peroxidation.

459   LD are known to protect non-transformed and transformed cells against a range

460 of cellular stresses typically encountered in the tumor microenvironment, including

461 nutrient deprivation and hypoxia (38,39). Indeed, these conditions induce LD formation

462 downstream of autophagy (30). Additionally, low pH up-regulates DGAT1 and

463 consequently increases LD formation. In turn, LD were required for acidosis-induced

464 metastasis (47). Nutrient deprivation and hypoxia compromise *de novo* FA synthesis

465 and desaturation. Unsaturated FA are essential for membrane fluidity and cell viability,

466 and in the absence of desaturation reactions, or the ability to scavenge unsaturated FA

467 from the circulation, cancer cells must draw on LD for unsaturated FA in order to survive

468 (48). The above role for LD is consistent with our observation that the effect of DGAT1

469 suppression on cell number was exacerbated by serum withdrawal and hypoxia and

470 explains why conversely DGAT1 overexpression conferred its greatest growth

471 advantage under these conditions.

472   Our data indicate that DGAT1 inhibition alone could be therapeutic in tumors

473   addicted to DGAT1, although diarrhea attendant on blocking fat absorption through the

474   gut (49) would have to be managed in patients. The identification of signaling molecules

475   such as SESN2, whose suppression synergized with DGAT1 antagonism to produce

476   high levels of ROS and significantly elevated cell death, might one-day feed into a

477   strategy that allows DGAT1 inhibitor concentration to be reduced to a well-tolerated

478   dose. Moreover, such pro-oxidant therapies could inhibit the progression of melanoma,

479   as oxidative stress limits melanoma metastasis (50).

480   Up-regulation of DGAT1 likely has additional profound consequences for cancer

481   progression, perhaps explaining the association between *DGAT1* amplification and

482   progression-free survival that we uncovered. Enhanced FA uptake and FAO are

483   particularly prominent in tumor initiating cells (9) and DGAT1 could play a critically

484   important role in this crucial subset of tumor cells. It was recently shown that FAO

485   activity correlates with antigen presentation in melanoma and responsiveness to

486   immune checkpoint immunotherapy (51). In fatty liver disease, lipid peroxide adducts

487   were shown to be highly immunogenic and drive adaptive immune responses (52). We

488   found that both substrate production for FAO and lipid peroxidation were suppressed by

489   DGAT1 up-regulation. Moreover, it has been found that LD are enriched with COX2 and

490   arachidonic acid and are major sites of PGE_2 synthesis (53). PGE_2 has wide ranging

491   suppressive effects on cellular immunity (54). Thus, DGAT1 up-regulation could

492   promote immune evasion by tumor cells and potentially diminish immunotherapy

493   responses; DGAT1 inhibitors might therefore synergize with immunotherapy.

494   Overall, our findings demonstrate that overexpression of the oncoprotein DGAT1,

495   with or without gene amplification, is a beneficial adaptation of cancer cells. DGAT1

496   overexpression permits accumulation of fatty acids, useful as an energy source, for

497   lipogenesis and for signal transduction, while avoiding suppression of growth factor

498   signaling and induction of oxidative stress.

499

ACKNOWLEDGEMENTS

511

512   **Author Contributions:** Cell line-based experimentation: DJW, MPS, RO, JH. Zebrafish

513   models: APB, DJW, HJ, MG, CC. Proteomics: MPS, DJW, PF, CF. Lipidomics: DJW,

514   MPS, ADS, DR, AJ, GRL, WBD. Bio-informatics analysis: DJW, SO, JW, HF, CF, ADS,

515   AJ, GRL, DR, WBD, MPS. Experimental design: DJW, APB, CF, MPS, AH. Sample

516   acquisition and cell lines: PL, CW, MPS, AH. Conceptualization: APB, MPS, AH.

517   Drafting manuscript: DJW, APB, MPS, AH. Revisions by all authors. Acquisition of

518   funds: CW, CF, AH. Study supervision MPS, AH.

519

520   **Competing interest:** No competing interests to declare.

521

522   **Supplementary Materials** contains supplemental methods, figures and tables.

523

Methods

Zebrafish models

526   Regulated procedures involving zebrafish were ethically approved by The University of

527   Manchester Animal Welfare and Ethical Review Body (AWERB), or by the UMMS

528   Institution Animal Care and Use Committee (A-2016, A-2171), and carried out under a

529   licence issued by the appropriate national regulatory authority. Zebrafish were housed

530   at ~28 °C under a 14 h light/10 h dark cycle. Transgenic zebrafish expressing

531    $BRAF^{V600E}$ or $NRAS^{G12D}$ have been previously described (28,55) and were crossed onto

532   a $mitfa^{w2/w2}$ ($mitfa^{-/-}$) background to suppress melanocyte development and further onto

533   a $tp53^{M214K/M214K}$ background to promote tumorigenesis. Melanocyte restoration and

534   simultaneous over-expression of Dgat1a, Dgat2 or EGFP was then achieved by

535   injection of embryos with a mitfa-minigene containing plasmid as previously described

536   (28). Briefly, zebrafish $dgat1a$ and $dgat2$ were amplified from cDNA of wild-type 48 h

537   post-fertilisation zebrafish embryos, and subcloned into the pDONR221 vector (see

538   Supplementary Table 8 for oligonucleotide sequences). The pDest-mitfa:dgat1a-pA and

539   pDest-mitfa:dgat2-pA destination vectors were created using an LR clonase reaction

23

540 consisting of p5E-mitfap, pME-dgat1a or pME-dgat2, p3E-pA and an empty destination

541 vector. Expression plasmid was injected into zebrafish zygotes along with Tol2 mRNA.

542 pCS2-TP plasmid for Tol2 mRNA generation was a kind gift from Dr Koichi Kawakami

543 (National Institute of Genetics). Sufficient embryos for all experimental arms were

544 generated simultaneously, pooled and then randomly assigned to a construct, although

545 formal randomization techniques were not used. Zebrafish were group-housed

546 according to the construct. Only zebrafish embryos with near complete melanocyte

547 rescue at 5 days were retained for further analysis. Analysis of tumor formation was not

548 performed blinded to the construct identity. Sample sizes were not predetermined based

549 on statistical power calculations but were based on our experience with these assays.

550 To assess the statistical significance of differences in overall survival, we used Mantel–

551 Cox's log-rank tests.

552

553 **Cell Lines**

554 Human melanoma cell lines were cultured in High Glucose DMEM with 10 % FBS, and

555 penicillin–streptomycin (Sigma) at 37 °C and 5 % CO_2. Normal human melanocytes

556 were purchased from Cascade Biologics and cultured according to manufacturer´s

557 guidelines. Lenti-X cells were cultured in High Glucose DMEM with 10 %v/v FBS, and

558 penicillin–streptomycin (Sigma) at 37 °C and 5 % CO_2. All cells tested negative for

559 mycoplasma and cell lines were authenticated using STR profiling.

Cell line	Genetic drivers	DGAT1 status
888MEL	BRAF^{V600E}	DGAT1 low
SKMEL28	BRAF^{V600E}	DGAT1 medium
SKMEL2	NRAS^{Q61R}	DGAT1 over expressed
MM485	NRAS^{Q61R}	DGAT1 over expressed
A375	BRAF^{V600E}	DGAT1 over expressed

SKMEL105	BRAF^{V600E}	DGAT1 over expressed
LOXIMVI	BRAF^{V600E}	DGAT1 amplified
SKMEL5	BRAF^{V600E}	DGAT1 amplified

560

Compounds and Antibodies

562 Compounds were used at the following concentrations unless otherwise noted 50 µM

563 AZD3988 (Tocris), 30 µM A922500 (Stratech) 50 µM AZD7687, 70 µM T863 (Sigma), 1

564 µM Oligomycin (Sigma), 0.5 µM FCCP (Sigma), 1 µM Antimycin-A (Sigma), 1 µM

565 Rotenone (Sigma), 50 µM PF-06424439 (Sigma), 5 µM Ebselen (Tocris), 1 mM Tempol,

566 200 µM Paraquat (Sigma), Menadione (Sigma), 100 µM Etomoxir (Sigma), 1 µM

567 LY2584702 (Stratech), 10 µM PF-4708671 (Generon).

568 Antibodies against DGAT1 (ab54037), phospho-PDE1a (ab92696) and 4-

569 Hydroxynonenal (ab46545) were purchased from abcam. Antibodies against Vinculin

570 (66305-1-Ig), Beta-Tubulin (10094-1-AP), PINK1 (23274-1-AP), Parkin (14060-1-AP),

571 SOD1 (10269-1-AP), SOD2 (24127-1-AP), Sestrin 2 (10795-1-AP), GAPDH (60004-1-

572 Ig), and PDK4 (12949-1-AP) were purchased from Proteintech. Antibodies against

573 phospho-S6 (2215), phospo-eEF2 (2331), phospho-AMPK (50081), phospho-RAPTOR

574 (2083), Caspase-3 (9662), phospho-P70 S6 kinase (9206), P70 S6 Kinase (2708), S6

575 (2317) and GFP (2956) were purchased from Cell Signalling. The Antibody against HA

576 (901533) was purchased from Biolegend. The Antibody against gamma-tubulin (T5326)

577 was purchased from Sigma.

578

Plasmids & siRNA

580 All plasmids were transfected using Lipofectamine (Invitrogen) following standard

581 protocols. The plasmids used were purchased from Addgene: pRK7-HA-S6K1-WT

582   (8984); pRK7-HA-S6K1-F5A-E389-deltaCT (8990); pcDNA3.1-mMaroon1 (83840). The

583   GFP and WPRE elements were excised from pCDH-MCS-T2A-copGFP (a kind gift from

584   Andrew Gilmore, The University of Manchester) using BspEI and KpnI. mApple (BspEI

585   and XhoI adapters) and WPRE (XhoI-KpnI adapters) were PCR amplified, digested and

586   subcloned to create the pCDH-MCS-T2A-mApple vector (see Supplementary Table 8

587   for oligonucleotide sequences). DGAT1 was further subcloned into the both the

588   pCDNA3.1 vector and pCDH-MCS-T2A-mApple using the MCS.

589   All siRNA was transfected using Lipofectamine RNAi Max (Invitrogen) following

590   standard protocols. The following siRNA were ordered from Dharmacon: DGAT1 007 5'

591   UCAAGGACAUGGACUACUC 3'; DGAT1 008 5' GCUGUGGUCUUACUGGUUG 3';

592   DGAT1 smart pool #J-009333-00-0005; DGAT2 01 5' GAACACACCCAAGAAAGGU 3';

593   DGAT2   02   5'GGAGGUAUCUGCCCUGUCA3';   DGAT2   03   5'

594   UCAUGGAGCUGACCUGGUU 3'; DGAT2 04 5'GAAUGCCUGUGUUGAGGGA 3';

595   DGAT2 smart pool #J-009333-08; SESN2 19 5'GGAGGGAGUAUUAGAUUAU3';

596   SESN2 20 5'GCAGGGACCCGUUGAACAA3'. The scrambled control siRNA (SIC002)

597   was ordered from Sigma.

598

599   **Viral transduction**

600   Briefly, Lenti-X cells were transfected with pMDLg/pRRE, pMD2.G, pRSV-Rev plasmids

601   (all kind gifts from Angeliki Malliri, Cancer Research UK Manchester Institute) and

602   pCDH-EF1α-DGAT1-T2A-mApple viral vectors using Fugene (Promega) following

603   standard protocols. The viral containing supernatant was filtered using a 0.45 μm filter

604   and frozen at –80 °C prior to transduction of target cells. The supernatant containing the

26

605   viral particles was added to target cells along with 10 ng/ml Polybrene (Millipore) for 24

606   h. Target cells were then grown and selected from single cell colonies.

607

608   **Protein lysate preparation and Western Blotting**

609   Cells were washed with PBS and lysed with sample buffer (62.5 mM TRIS pH 6.8, 2

610   %w/v Sodium dodecyl sulfate (SDS), 10 %v/v glycerol, 0.01%w/v bromophenol blue, 3

611   %v/v 2-mercaptoethanol). Lysates were then sonicated and heated to 95°C for 10

612   minutes prior to being evenly loaded onto SDS-polyacrylamide gels using the Mini

613   Trans-Bot electrophoresis system (Biorad), followed by transfer to PVDF using standard

614   western blotting procedures.

615

616   **Lipid droplet staining and image analysis**

617   ***Bodipy 493/503***

618   Indicated cells were stained with 2 μM Bodipy 493/503 (ThermoFisher Scientific) and 5

619   ng/ml Hoecsht 3342 (Cell Signalling) for 30 minutes prior to fixing in 4 %w/v

620   paraformaldehyde and imaging using a Leica microscope system. Images were

621   processing using Fiji.

622   ***Lipidtox***

623   Indicated cells were fixed in 4 %w/v paraformaldehyde and stained with LipidTox Green

624   (ThermoFisher Scientific) according to manufacturer's instructions, and 5ng/ml Hoecsht

625   3342 (Cell Signalling) for 15 minutes prior to imaging using a Leica microscope system.

626   Images were processing using Fiji.

627

RNA Isolation and real-time PCR analysis

RNA from cell lines was isolated with TRIZOL® (Invitrogen). After chloroform extraction and centrifugation, 5 µg RNA was DNase treated using RNase-Free DNase Set (Qiagen). 1 µg of DNase treated RNA was then taken for cDNA synthesis using the Protoscript I first strand cDNA synthesis kit (New England Biolabs). Selected genes were amplified by quantitative real time PCR (RT-qPCR) using Sygreen (PCR Biosystems). Relative expression was calculated using the delta-delta CT methodology and beta-actin was used as reference housekeeping gene. Sequences for primers used can be found in the Supplementary Table 8.

Incucyte cell-proliferation assay and apoptosis assay

Indicated cell lines were seeded into 24-well plates at a density of 15,000–20,000 cells per well, depending on growth rate and the design of the experiment. After 24 h drugs or siRNA were added and cells were imaged every hour using the Incucyte ZOOM (Essen Bioscience) Phase-contrast images were analysed to detect cell proliferation based on cell confluence. For cell apoptosis, caspase-3 and caspase-7 green apoptosis-assay reagent (Life Technologies) was added to the culture medium following manufacturer's instructions. Cell apoptosis was analysed based on green fluorescent staining of apoptotic cells.

Flow cytometry

Mitochondrial Membrane potential

650   Indicated cell lines were trypzinized and pelleted by centrifugation at 500 g for 5 min,

651   washed with PBS. For mitochondrial membrane potential cells were stained with 2 µM

652   JC-1 (Life Technologies) for 30 minutes at 37 °C. For positive control samples 0.5µM

653   FCCP was added simultaneously with JC-1. Data was acquired by the BD BIOsciences

654   Foretessa and quantified using the Flowjo software. A minimum of 10,000 cells were

655   analysed per condition.

656

657   ***Lipid peroxidation***

658   Indicated cell lines were trypzinized and pelleted by centrifugation at 500 g for 5 min,

659   followed by a PBS wash. For lipid peroxidation cells were stained with either 5 µM

660   BODIPY™ 581/591 C11 (ThermoFisher Scientific) or MitoPerOx (Abcam) for 30

661   minutes at 37 °C. Data was acquired by the BD BIOsciences Foretessa and quantified

662   using the Flowjo software. A minimum of 10,000 cells were analysed per condition.

663

664   ***Mitochondrial ROS***

665   Indicated cell lines were trypzinized and pelleted by centrifugation at 500 g for 5 min,

666   followed by a PBS wash. For mitochondrial specific ROS detection, cells were stained

667   with 2.5 µM Mitosox (ThermoFisher Scientific) for 30 minutes at 37 °C. Data was

668   acquired by the BD BIOsciences Foretessa and quantified using the Flowjo software. A

669   minimum of 10,000 cells were analysed per condition.

670

671   **Proliferation Assays**

672   ***Crystal Violet***

673 Indicated cells were stained and fixed with 0.5 %w/v crystal violet (Sigma) in 4 %w/v

674 paraformaldehyde/PBS for 30 minutes. Fixed cells were then solubilised in 2 %w/v

675 SDS/PBS and absorbance measured at 595 nm using Synergy H1 microplate reader

676 (BioTek).

677 *EdU Incorporation*

678 Indicated cells were labelled with 20 µM 5-ethynyl-2'-deoxyuridine (EdU) for 4 h and

679 processed following the manufacturer's protocol (Click-iT® EdU Alexa Fluor® 488

680 Imaging Kit, Thermo Fisher). Prior to imaging cells were then stained with 5ng/ml

681 Hoecsht 3342 for 15 minutes. Stained cells were analysed using a using a Leica

682 microscope system. Images were processing using Fiji.

683

684 **Dihydroethidium Assay**

685 Cells were stained with 5 µM Dihydroethidium for 20 minutes in the dark at 37 °C.

686 Fluorescence was measured at excitation 480nm emission 570 nm using Synergy H1

687 micro plate reader (BioTek). Fluorescence values were normalised to cell number by

688 staining the cells with crystal violet after fluorescence read.

689

690 **Cancer bioinformatics**

691 We evaluated both point mutations and CNV in the TCGA SKCM firehose legacy,

692 TCGA pan-cancer and Cancer Cell Line Encyclopedia datasets using the cBioPortal

693 platform (56). The GISTIC2.0 algorithm was used to identify focal amplifications (57).

694 Gene Ontology analysis was carried out using both enrichR (58) and metascape

695 software (59). Association between mRNA expression in TCGA datasets and survival

696   was evaluated using OncoLnc (60). mRNA levels determined by microarray were

697   accessed through the Oncomine platform (61).

698

699   **Quantification and Statistical Analysis**

700   Data was tested for normality using the Shapiro-Wilk test. Data was considered to be

701   normally distributed if $p > 0.05$. Differences in the number of lipid droplets per cell,

702   relative cell number and percentage EdU incorporation between DMSO and drug

703   treated cells were assessed using an unpaired two-sided *t*-test, or Mann-Whitney test if

704   data were not normally distributed. In comparing the differences in these same

705   characteristics between cells transfected with either non-target or one of several siRNA

706   oligonucleotides, a one-way ANOVA with Tukey's multiple comparisons test (or

707   Friedman with Dunn's multiple comparisons test if data were not normally distributed)

708   was used to measure significance. Differences were considered significant if $p < 0.05$. All

709   data obtained was analysed using Graphpad Prism 8.1.

710

711   **Data and Code Availability**

712   The zebrafish tumor RNA-seq data has been deposited with the Gene Expression

713   Omnibus (GEO) with the accession code GSE144555. The mass spectrometry

714   proteomics data have been deposited with the ProteomeXchange Consortium via the

715   PRIDE partner repository with the dataset identifier PXD017487. Extended Lipidomics

716   Data for zebrafish tumors and human melanoma cell lines can be found in

717   Supplementary Tables 3-7. Code for proteomic analysis can be found at

718   https://github.com/JoWatson2011/DGAT_2019.

31

719

REFERENCES

720 **REFERENCES**

721 1.   DeBerardinis RJ, Chandel NS. Fundamentals of cancer metabolism. Sci Adv

722   **2016**;2:e1600200-e

723 2.   Andrejeva G, Rathmell JC. Similarities and Distinctions of Cancer and Immune

724   Metabolism in Inflammation and Tumors. Cell Metabolism **2017**;26:49-70

725 3.   Lee SY, Ju MK, Jeon HM, Lee YJ, Kim CH, Park HG, *et al.* Oncogenic

726   Metabolism Acts as a Prerequisite Step for Induction of Cancer Metastasis and

727   Cancer Stem Cell Phenotype. Oxid Med Cell Longev **2018**;2018:1027453-

728 4.   Lyssiotis CA, Kimmelman AC. Metabolic Interactions in the Tumor

729   Microenvironment. Trends Cell Biol **2017**;27:863-75

730 5.   Koundouros N, Poulogiannis G. Reprogramming of fatty acid metabolism in

731   cancer. British Journal of Cancer **2020**;122:4-22

732 6.   Chen M, Huang J. The expanded role of fatty acid metabolism in cancer: new

733   aspects and targets. Precis Clin Med **2019**;2:183-91

734 7.   Lengyel E, Makowski L, DiGiovanni J, Kolonin MG. Cancer as a Matter of Fat:

735   The Crosstalk between Adipose Tissue and Tumors. Trends Cancer **2018**;4:374-

736   84

737 8.   Watt MJ, Clark AK, Selth LA, Haynes VR, Lister N, Rebello R, *et al.* Suppressing

738   fatty acid uptake has therapeutic effects in preclinical models of prostate cancer.

739   Science Translational Medicine **2019**;11:eaau5758

740   9.   Pascual G, Avgustinova A, Mejetta S, Martin M, Castellanos A, Attolini CS, *et al.*

741   Targeting metastasis-initiating cells through the fatty acid receptor CD36. Nature

742   **2017**;541:41-5

743   10.   Nieman KM, Kenny HA, Penicka CV, Ladanyi A, Buell-Gutbrod R, Zillhardt MR,

744   *et al.* Adipocytes promote ovarian cancer metastasis and provide energy for rapid

745   tumor growth. Nature Medicine **2011**;17:1498-503

746   11.   Maan M, Peters JM, Dutta M, Patterson AD. Lipid metabolism and lipophagy in

747   cancer. Biochemical and Biophysical Research Communications **2018**;504:582-9

748   12.   Nomura DK, Long JZ, Niessen S, Hoover HS, Ng S-W, Cravatt BF.

749   Monoacylglycerol Lipase Regulates a Fatty Acid Network that Promotes Cancer

750   Pathogenesis. Cell **2010**;140:49-61

751   13.   Brookheart RT, Michel CI, Schaffer JE. As a matter of fat. Cell metabolism

752   **2009**;10:9-12

753   14.   Molenaar RJ, Maciejewski JP, Wilmink JW, van Noorden CJF. Wild-type and

754   mutated IDH1/2 enzymes and therapy responses. Oncogene **2018**;37:1949-60

755   15.   Flavin R, Peluso S, Nguyen PL, Loda M. Fatty acid synthase as a potential

756   therapeutic target in cancer. Future Oncol **2010**;6:551-62

757   16.   Martín-Martín N, Carracedo A, Torrano V. Metabolism and Transcription in

758   Cancer: Merging Two Classic Tales. Front Cell Dev Biol **2018**;5:119-

759   17.   Rodríguez-Enríquez S, Marín-Hernández Á, Gallardo-Pérez CJ, Pacheco-

760   Velázquez CS, Belmont-Díaz AJ, Robledo-Cadena XD, *et al.* Transcriptional

761   Regulation of Energy Metabolism in Cancer Cells. Cells **2019**;8

762   18.   van Rooijen E, Fazio M, Zon LI. From fish bowl to bedside: The power of

763   zebrafish to unravel melanoma pathogenesis and discover new therapeutics.

764   Pigment Cell & Melanoma Research **2017**;30:402-12

765   19.   Henderson F, Johnston HR, Badrock AP, Jones EA, Forster D, Nagaraju RT*, et*

766   *al.* Enhanced Fatty Acid Scavenging and Glycerophospholipid Metabolism

767   Accompany Melanocyte Neoplasia Progression in Zebrafish. Cancer Res

768   **2019**;79:2136-51

769   20.   Wilfling F, Wang H, Haas JT, Krahmer N, Gould TJ, Uchida A*, et al.*

770   Triacylglycerol synthesis enzymes mediate lipid droplet growth by relocalizing

771   from the ER to lipid droplets. Dev Cell **2013**;24:384-99

772   21.   DeVita RJ, Pinto S. Current Status of the Research and Development of

773   Diacylglycerol O-Acyltransferase 1 (DGAT1) Inhibitors. Journal of Medicinal

774   Chemistry **2013**;56:9820-5

775   22.   Zhang M, Di Martino JS, Bowman RL, Campbell NR, Baksh SC, Simon-Vermot

776   T*, et al.* Adipocyte-Derived Lipids Mediate Melanoma Progression via FATP

777   Proteins. Cancer Discov **2018**;8:1006-25

778   23.   Fischer GM, Vashisht Gopal YN, McQuade JL, Peng W, DeBerardinis RJ, Davies

779   MA. Metabolic strategies of melanoma cells: Mechanisms, interactions with the

780   tumor microenvironment, and therapeutic implications. Pigment Cell Melanoma

781   Res **2018**;31:11-30

782   24.   Venkatesan AM, Vyas R, Gramann AK, Dresser K, Gujja S, Bhatnagar S*, et al.*

783   Ligand-activated BMP signaling inhibits cell differentiation and death to promote

784   melanoma. J Clin Invest **2018**;128:294-308

785   25.   Schlagbauer-Wadl H, Griffioen M, van Elsas A, Schrier PI, Pustelnik T, Eichler

786   HG, *et al.* Influence of increased c-Myc expression on the growth characteristics

787   of human melanoma. J Invest Dermatol **1999**;112:332-6

788   26.   Ehlers JP, Worley L, Onken MD, Harbour JW. DDEF1 is located in an amplified

789   region of chromosome 8q and is overexpressed in uveal melanoma. Clin Cancer

790   Res **2005**;11:3609-13

791   27.   Bastian BC, LeBoit PE, Hamm H, Brocker EB, Pinkel D. Chromosomal gains and

792   losses in primary cutaneous melanomas detected by comparative genomic

793   hybridization. Cancer Res **1998**;58:2170-5

794   28.   Ceol CJ, Houvras Y, Jane-Valbuena J, Bilodeau S, Orlando DA, Battisti V, *et al.*

795   The histone methyltransferase SETDB1 is recurrently amplified in melanoma and

796   accelerates its onset. Nature **2011**;471:513-7

797   29.   Ackerman D, Simon MC. Hypoxia, lipids, and cancer: surviving the harsh tumor

798   microenvironment. Trends in Cell Biology **2014**;24:472-8

799   30.   Nguyen TB, Louie SM, Daniele JR, Tran Q, Dillin A, Zoncu R, *et al.* DGAT1-

800   Dependent Lipid Droplet Biogenesis Protects Mitochondrial Function during

801   Starvation-Induced Autophagy. Dev Cell **2017**;42:9-21 e5

802   31.   Falomir-Lockhart LJ, Cavazzutti GF, Giménez E, Toscani AM. Fatty Acid

803   Signaling Mechanisms in Neural Cells: Fatty Acid Receptors. Frontiers in Cellular

804   Neuroscience **2019**;13

805   32.   Zhang S, Hulver MW, McMillan RP, Cline MA, Gilbert ER. The pivotal role of

806   pyruvate dehydrogenase kinases in metabolic flexibility. Nutrition & Metabolism

807   **2014**;11:10

808   33.   Koves TR, Ussher JR, Noland RC, Slentz D, Mosedale M, Ilkayeva O*, et al.*

809   Mitochondrial Overload and Incomplete Fatty Acid Oxidation Contribute to

810   Skeletal Muscle Insulin Resistance. Cell Metabolism **2008**;7:45-56

811   34.   Sajadimajd S, Khazaei M. Oxidative Stress and Cancer: The Role of Nrf2. Curr

812   Cancer Drug Targets **2018**;18:538-57

813   35.   Conrad M, Pratt DA. The chemical basis of ferroptosis. Nat Chem Biol

814   **2019**;15:1137-47

815   36.   Pasha M, Eid AH, Eid AA, Gorin Y, Munusamy S. Sestrin2 as a Novel Biomarker

816   and Therapeutic Target for Various Diseases. Oxid Med Cell Longev

817   **2017**;2017:3296294-

818   37.   Guri Y, Colombi M, Dazert E, Hindupur SK, Roszik J, Moes S*, et al.* mTORC2

819   Promotes Tumorigenesis via Lipid Synthesis. Cancer Cell **2017**;32:807-23.e12

820   38.   Cruz ALS, Barreto EdA, Fazolini NPB, Viola JPB, Bozza PT. Lipid droplets:

821   platforms with multiple functions in cancer hallmarks. Cell Death & Disease

822   **2020**;11:105

823   39.   Petan T, Jarc E, Jusović M. Lipid Droplets in Cancer: Guardians of Fat in a

824   Stressful World. Molecules **2018**;23

825   40.   Saxton RA, Sabatini DM. mTOR Signaling in Growth, Metabolism, and Disease.

826   Cell **2017**;168:960-76

827   41.   Foster DA. Phosphatidic acid and lipid-sensing by mTOR. Trends Endocrinol

828   Metab **2013**;24:272-8

829   42.   Schmitz-Peiffer C, Biden TJ. Protein kinase C function in muscle, liver, and beta-

830   cells and its therapeutic implications for type 2 diabetes. Diabetes **2008**;57:1774-

831   83

832   43.   Porstmann T, Santos CR, Griffiths B, Cully M, Wu M, Leevers S, *et al.* SREBP

833   Activity Is Regulated by mTORC1 and Contributes to Akt-Dependent Cell

834   Growth. Cell Metabolism **2008**;8:224-36

835   44.   Lee G, Zheng Y, Cho S, Jang C, England C, Dempsey JM, *et al.* Post-

836   transcriptional Regulation of De Novo Lipogenesis by mTORC1-S6K1-SRPK2

837   Signaling. Cell **2017**;171:1545-58.e18

838   45.   Gaschler MM, Stockwell BR. Lipid peroxidation in cell death. Biochemical and

839   biophysical research communications **2017**;482:419-25

840   46.   Jarc E, Kump A, Malavašič P, Eichmann TO, Zimmermann R, Petan T. Lipid

841   droplets induced by secreted phospholipase A2 and unsaturated fatty acids

842   protect breast cancer cells from nutrient and lipotoxic stress. Biochimica et

843   Biophysica Acta (BBA) - Molecular and Cell Biology of Lipids **2018**;1863:247-65

844   47.   Corbet C, Bastien E, Santiago de Jesus JP, Dierge E, Martherus R, Vander

845   Linden C, *et al.* TGFbeta2-induced formation of lipid droplets supports acidosis-

846   driven EMT and the metastatic spreading of cancer cells. Nat Commun

847   **2020**;11:454

848   48.   Ackerman D, Tumanov S, Qiu B, Michalopoulou E, Spata M, Azzam A, *et al.*

849   Triglycerides Promote Lipid Homeostasis during Hypoxic Stress by Balancing

850   Fatty Acid Saturation. Cell Rep **2018**;24:2596-605.e5

851 49. Denison H, Nilsson C, Lofgren L, Himmelmann A, Martensson G, Knutsson M*, et*

852 *al.* Diacylglycerol acyltransferase 1 inhibition with AZD7687 alters lipid handling

853 and hormone secretion in the gut with intolerable side effects: a randomized

854 clinical trial. Diabetes Obes Metab **2014**;16:334-43

855 50. Piskounova E, Agathocleous M, Murphy MM, Hu Z, Huddlestun SE, Zhao Z*, et*

856 *al.* Oxidative stress inhibits distant metastasis by human melanoma cells. Nature

857 **2015**;527:186-91

858 51. Harel M, Ortenberg R, Varanasi SK, Mangalhara KC, Mardamshina M, Markovits

859 E*, et al.* Proteomics of Melanoma Response to Immunotherapy Reveals

860 Mitochondrial Dependence. Cell **2019**;179:236-50 e18

861 52. Sutti S, Jindal A, Locatelli I, Vacchiano M, Gigliotti L, Bozzola C*, et al.* Adaptive

862 immune responses triggered by oxidative stress contribute to hepatic

863 inflammation in NASH. Hepatology **2014**;59:886-97

864 53. D'Avila H, Melo RCN, Parreira GG, Werneck-Barroso E, Castro-Faria-Neto HC,

865 Bozza PT. Mycobacterium bovis Bacillus Calmette-Guérin

866 Induces TLR2-Mediated Formation of Lipid Bodies: Intracellular Domains for

867 Eicosanoid Synthesis In Vivo. The Journal of Immunology **2006**;176:3087

868 54. Kalinski P. Regulation of Immune Responses by Prostaglandin

869 E₂. The Journal of Immunology **2012**;188:21

870 55. Casar B, Badrock AP, Jimenez I, Arozarena I, Colon-Bolea P, Lorenzo-Martin

871 LF*, et al.* RAS at the Golgi antagonizes malignant transformation through

872 PTPRkappa-mediated inhibition of ERK activation. Nat Commun **2018**;9:3595

873   56.   Gao J, Aksoy BA, Dogrusoz U, Dresdner G, Gross B, Sumer SO*, et al.*

874   Integrative analysis of complex cancer genomics and clinical profiles using the

875   cBioPortal. Sci Signal **2013**;6:pl1

876   57.   Mermel CH, Schumacher SE, Hill B, Meyerson ML, Beroukhim R, Getz G.

877   GISTIC2.0 facilitates sensitive and confident localization of the targets of focal

878   somatic copy-number alteration in human cancers. Genome Biology

879   **2011**;12:R41

880   58.   Chen EY, Tan CM, Kou Y, Duan Q, Wang Z, Meirelles GV*, et al.* Enrichr:

881   interactive and collaborative HTML5 gene list enrichment analysis tool. BMC

882   Bioinformatics **2013**;14:128

883   59.   Zhou Y, Zhou B, Pache L, Chang M, Khodabakhshi AH, Tanaseichuk O*, et al.*

884   Metascape provides a biologist-oriented resource for the analysis of systems-

885   level datasets. Nature Communications **2019**;10:1523

886   60.   Anaya J. OncoLnc: linking TCGA survival data to mRNAs, miRNAs, and

887   lncRNAs. Peerj Comput Sci **2016**

888   61.   Rhodes DR, Yu J, Shanker K, Deshpande N, Varambally R, Ghosh D*, et al.*

889   ONCOMINE: a cancer microarray database and integrated data-mining platform.

890   Neoplasia **2004**;6:1-6

891

892

893 **Figure 1 *DGAT1* amplification and up-regulation is associated with poor**

894 **prognosis in melanoma**

895 (a) Patient survival from TCGA melanoma cohort (25% top vs 75% bottom by mRNA

896 abundance, Y-axis) *versus* fold-change in mRNA expression of lipid metabolism genes

897 in zebrafish tumors (X-axis). (b) Kaplan-Meier survival plot comparing melanoma

898 patients based on expression of *DGAT1* or *DGAT2* (top 25% *vs* bottom 75%, TCGA

899 data set). (c) *DGAT1* relative gene expression in skin, nevi and melanoma tumors from

900 indicated studies (Mean ± SD, n>3). (d) Protein expression of DGAT1 and Vinculin

901 (loading control) (NHM- Normal Human Melanocytes). (e) Genetic alterations in the

902 TCGA firehose legacy melanoma data set (counting only samples with CNV data)

903 obtained from cBioPortal. (f) Schematic depicting human chromosome 8, the amplified

904 arm (red), and known/putative melanoma oncogenes within this region. (g) G-Score of

905 amplified regions of zebrafish chromosomes found in *BRAF^{V600E}*-positive; *tp53* mutant

906 tumors indicating the position of presumed melanoma oncogene homologues. (h)

907 Kaplan-Meier progression free survival plot comparing patients across multiple cancer

908 types based on *DGAT1* amplification.

909

910 **Figure 2 Dgat1 functions as an oncoprotein in zebrafish**

911 (a) *DGAT1* amplification distribution in melanoma. (b) Kaplan-Meier plot of melanoma

912 tumor nodule incidence in EGFP control or Dgat1a over-expressing animals on the *tp53*

913 mutant; *nacre* genetic background. Representative images shown for EGFP and Dgat1a

40

914   positive animals at 54 and 76 weeks post-fertilisation respectively. (c) as for (b) but on

915   the transgenic *mitfa:BRAF^V600E^*; *tp53* mutant; *nacre* genetic background. Representative

916   images are shown at 12 weeks post fertilisation. (d) as for (c) but on the transgenic

917   *mitfa:NRAS^G12D^*; *tp53* mutant; *nacre* genetic background, also shown the effect of Dgat2

918   over-expression. (e) Hematoxylin and eosin stained transverse sections of EGFP

919   expressing or Dgat1a over-expressing melanoma on the transgenic *mitfa*:*NRAS*^G12D^;

920   *tp53* mutant; *nacre* genetic background. (f) Volcano plot of all genes from RNA-seq data

921   from NRAS^G12D^-positive EGFP-expressing (n=3) and from NRAS^G12D^-positive Dgat1a

922   over- expressing (n=5) tumors. Fold-change calculated comparing Dgat1a over-

923   expressing tumors to EGFP-expressing control tumors. (g) *DGAT1* expression in TGCA

924   pan cancer atlas RNA-seq data set filtered for NRAS^mut^ melanoma patients (upper).

925   Venn diagram of significantly enriched gene sets after GSEA of significantly regulated

926   genes comparing either NRAS^G12D^-positive EGFP-expressing (n=3) and NRAS^G12D^-

927   positive Dgat1a over-expressing (n=5) tumors or comparing DGAT1 mRNA high tumors

928   (12/72) to the rest of the NRAS^mut^ TGCA dataset (60/72). (h) Selection of 11 pathways

929   from the Venn diagram intersect is shown in the dot-plot. Dot size represents the *P*

930   value.

931

932   Figure 3 DGAT1 activity is required for maintenance of S6K signalling

933   (a) Phospho-proteomics work flow (left). Enriched phosphorylated sites (WebGestalt) of

934   up- (59) and down-regulated (96) phosphorylated proteins. Protein hub analysis of both

935   up- and down-regulated phosphorylated proteins (right) (n=3). (b) Protein expression of

41

936   phospho-S6 and phospho-eEF2 following DGAT1 inhibitor treatment. (c) Confluency

937   curves in cell lines transfected with DGAT1 targeting (007, 008, pool) or scrambled (SC)

938   siRNAs (Mean, n=3) (above). Corresponding protein expression of DGAT1, phospho-S6

939   and phospho-eEF2. (d) Confluency curves of parental 888MEL cells and 888mel cells

940   following lentiviral transduction with a DGAT1 over-expression vector and clonal

941   selection (Mean, n=3) (upper left). Corresponding crystal violet staining after 72 h

942   growth (upper right). Corresponding protein expression of DGAT1 and phospho-S6

943   (lower).

944

945   **Figure 4 DGAT1 supports S6K dependent melanoma cell growth**

946   (a) Heatmap of relative cell number determined by crystal violet following 72 h DGAT1

947   inhibitor treatment (Mean, n>3). (b) Percentage of cells in S-phase using EdU

948   incorporation following 24 h DGAT1 inhibitor treatment (Mean, n>3). (c) Protein

949   expression in SKMEL105 cells of HA-tag, DGAT1 and phospho-S6 following both over

950   expression of either GFP wild type S6 kinase or constitutively active S6-kinase and

951   transfection with a DGAT1 targeting or scrambled siRNA (left). Confluency curves of

952   SKMEL105 cells following both over-expression of S6 kinase or GFP and transfection

953   with a DGAT1 targeting or scrambled siRNA (Mean, n=3) (right). (d) Quantification of

954   the percentage of A375 cells in S-phase using EdU incorporation following over-

955   expression of either S6 kinase, constitutively active S6 kinase or a GFP control

956   with/without the presence of A922500 for 24 h (Mean ± SD, n>6). (e) Confluency

957   curves of 888MEL and clone 3 cells following treatment with/without 1 µM LY2584702

958   or 10 μM PF-4708671 determined by time-lapse microscopy using an Incucyte zoom

959   system (left) (Mean ± SD, n=4). Corresponding protein expression of phospho-P70S6K,

960   phospho-S6, S6 and DGAT1 (right). (f) Graph showing relative cell number determined

961   by crystal violet following 72 h DGAT1 inhibitor treatment with cells grown in varying

962   concentrations of foetal calf serum (FCS) (Mean, n>3). (g) Graph of relative cell number

963   determined by crystal violet following 48 h DGAT1 inhibitor treatment under normoxic or

964   hypoxic conditions (1% O2) with cells grown in varying concentrations of foetal calf

965   serum (FCS) (relative to DMSO control for each condition) (Mean, n>3).

966

967   Figure 5 DGAT1-driven lipid droplets act as caretakers of mitochondrial health

968   (a) Lipidomic profiling using UHPLC-MS of $NRAS^{G12D}$-positive EGFP-expressing (n=6)

969   and $NRAS^{G12D}$-positive Dgat1a-over-expressing (n=6) tumors showing the ratio of lipid

970   species (annotated by MS/MS). (b) Representative images of 888MEL and Clone 3

971   cells stained with BODIPY (left). Brightfield images of 888MEL parental cells and Clone

972   3 DGAT1 over-expressing cells (middle). UHPLC-lipidomic analysis of 888MEL parental

973   and Clone 3 DGAT1 over-expressing cells. Fold-change relative to 888MEL parental

974   cells (right). TAG (triacyclglycerides), AcCa (acyl carnitine). (c) Quantification of the

975   number of lipid droplets per cell using BODIPY staining following AZD3988 treatment

976   (Mean ± SD, n>30). (d) UHPLC-lipidomic analysis of SKMEL105 cells following

977   A922500 treatment. Fold-change relative to DMSO. TAG (triacyclglycerides), LPC

978   (lysophosphatidycholine), AcCa (acyl carnitine), LPE (lysophosphatidylethanolamine).

979   (e) Lipid species fold changes in SKMEL105 following 72 h A922500 treatment plotted

980 versus lipid species fold changes observed in clone 3 cells. f) Protein expression of

981 phospho-AMPK and phospho-RAPTOR following A922500 treatment. (g) Oxygen

982 consumption rate in A375 cells following 48 h A922500 treatment (upper). Basal

983 respiration, ATP production and spare respiratory capacity were calculated (lower)

984 (Mean ± SD, n=3). (h) Staining with JC-1 dye following A922500 treatment or following

985 transfection with DGAT1 targeting siRNA. The percentage of cells that lost red J-

986 aggregates was calculated by using 1 μM CCP as a positive control and comparing this

987 to untreated cells to create two populations of cells for flow cytometry analysis (upper)

988 (Mean ± SD, n>3). Protein expression of PINK1 and PARKIN following A922500

989 treatment (lower).

990

991 **Figure 6 DGAT1 suppression generates ROS leading to mitochondrial lipid**

992 **peroxidation**

993 (a) Total proteomics work flow (left). GEO of up-regulated proteins (114) ranked by

994 combined score (wikipathways) or log adjusted P values (metascape) (right) (b). RT-

995 qPCR analysis following A922500 treatment. Fold-change relative to DMSO (Mean,

996 n=3). (c) Quantification of ROS levels using dihydroethidium fluorescence following

997 A922500 treatment. Fold-change relative to DMSO (Mean, n>4). (d) Quantification of

998 ROS levels using dihydroethidium fluorescence following transfection with either

999 DGAT1 targeting siRNA or a scrambled control for 48-72 h. Fold-change calculated

1000 relative to scrambled control (Mean ± *S*D, n=3) (upper). Corresponding protein

1001 expression of DGAT1 and phospho-AMPK (lower). (e) C11-Bodipy staining following

44

1002   A922500 treatment. Median fluorescence determined using FACS (Median ± SD, n>6).

1003   (f) Mito-C11-Bodipy staining following A922500 treatment. Median fluorescence

1004   determined using FACS (Median ± SD, n>6) (left) Representative histogram of B530/30-

1005   A fluorescence (right). (g) Protein expression of DGAT1 and 4-Hydroxynonenal

1006   following transfection with either DGAT1 targeting siRNA or a scrambled control for 48

1007   h. (h) Protein expression of DGAT1 and 4-Hydroxynonenal following transfection with

1008   either DGAT1 over-expression vector or an empty vector control for 48 h. (i) Protein

1009   expression of Dgat1 , GFP and 4-Hydroxynonenal in $NRAS^{G12D}$-positive GFP-

1010   expressing (n=4) and $NRAS^{G12D}$-positive Dgat1a over-expressing (n=7) tumors.

1011

1012   **Figure 7 DGAT1 suppression triggers ROS induced apoptosis that is ameliorated**

1013   **by SESN2**

1014   (a) Protein expression of SOD1, SOD2 and cleaved caspase3 following A922500

1015   treatment. (b) Cleaved-caspase index following transfection of a DGAT1 targeting or

1016   scrambled siRNA. At 24 h cells were treated with/without Tempol or Ebselen (Mean,

1017   n=3) (lower). Corresponding protein expression of DGAT1 and cleaved caspase3

1018   (upper). (c) Drug-dose response curve after 72 h treatment with ROS inducers (upper)

1019   (Mean ± SD, n=*3*). Protein expression of cleaved-caspase3 and DGAT1 following 72 h

1020   paraquat treatment (lower). (d) Relative cell number determined using crystal violet

1021   staining following 48 h culture in indicated FCS serum levels under hypoxic (1% O2) or

1022   normoxic conditions (Mean ± SEM, n>3) (Upper). Corresponding protein expression of

1023   SOD2, DGAT1 and cleaved caspase 3 under hypoxic (1% O2) conditions (lower). (e)

45

1024   Protein expression of SESN2 following A922500 treatment. (f) Confluency curves of

1025   A375 cells transfected with either SESN2 or DGAT1 targeting or scrambled siRNA (left).

1026   Corresponding cleaved-caspase index (right). Corresponding protein expression of

1027   DGAT1 and Sestrin 2 (lower). (g) Quantification of ROS levels using dihydroethidium

1028   fluorescence in A375 cells transfected with SESN2 targeting or scrambled siRNA (19,

1029   20) followed by A922500 treatment for 24 h. Fold-change relative to scrambled control

1030   (Mean ± SD, n>4). (h) Relative HMOX1 expression in A375 cells transfected with

1031   SESN2 targeting or scrambled siRNA (19, 20) followed by A922500 treatment for 24 h.
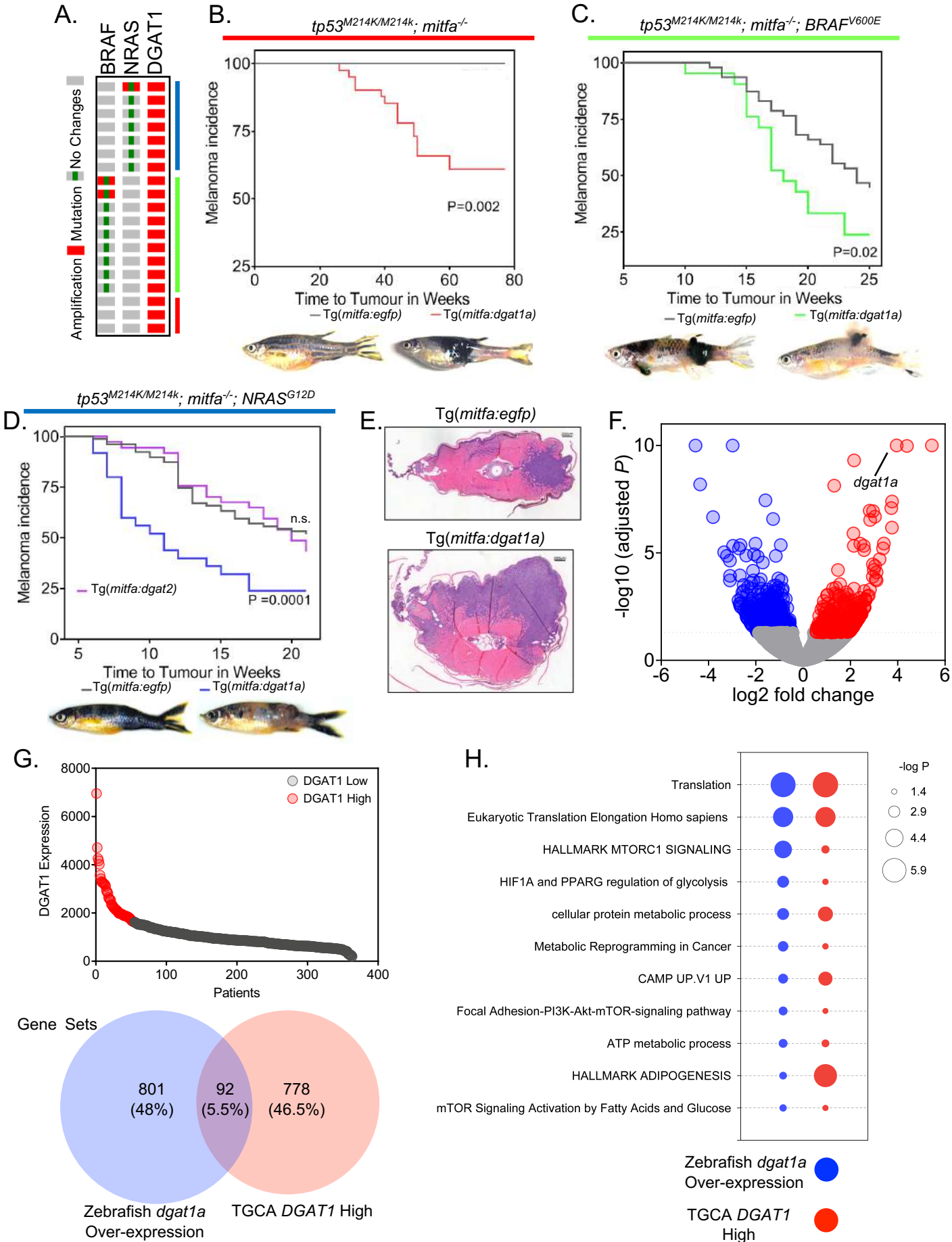
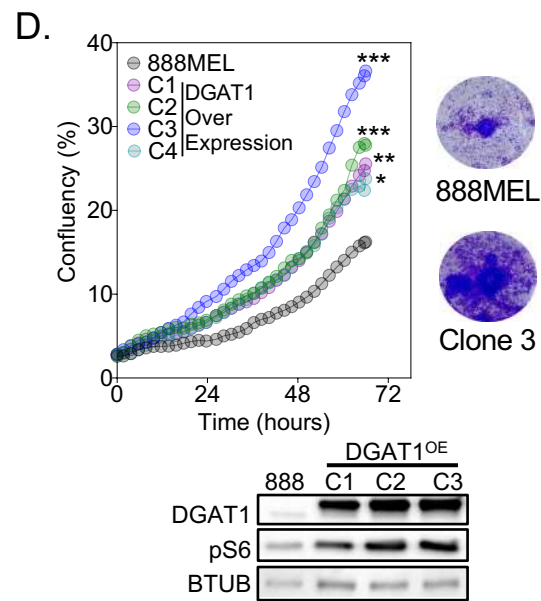1032   Fold-change relative to DMSO (Mean ± SD, n=3).
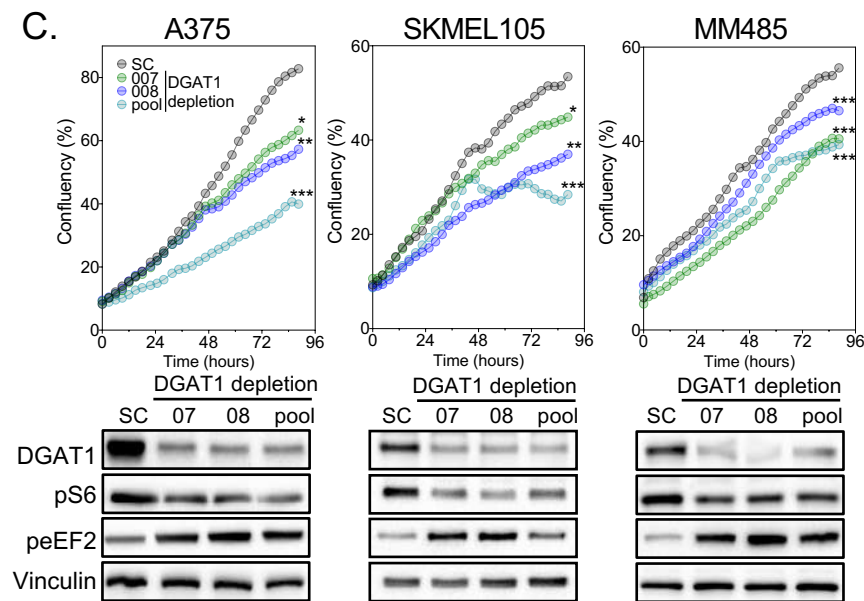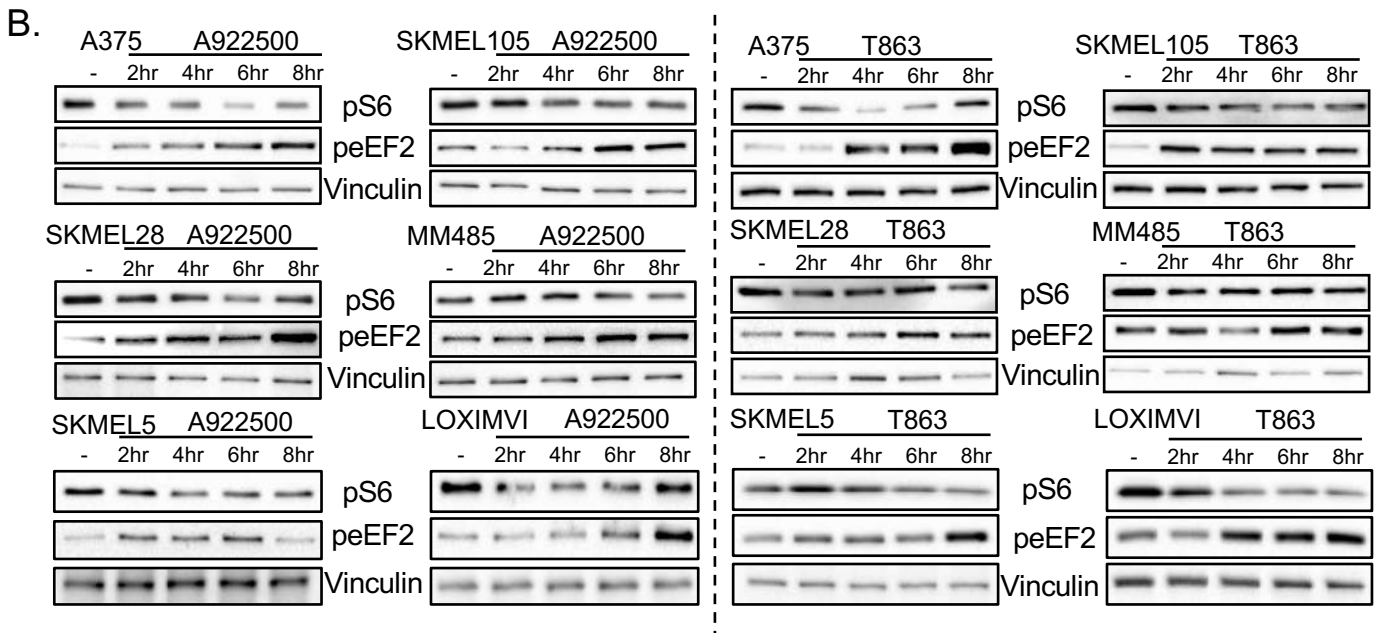
1033

1034
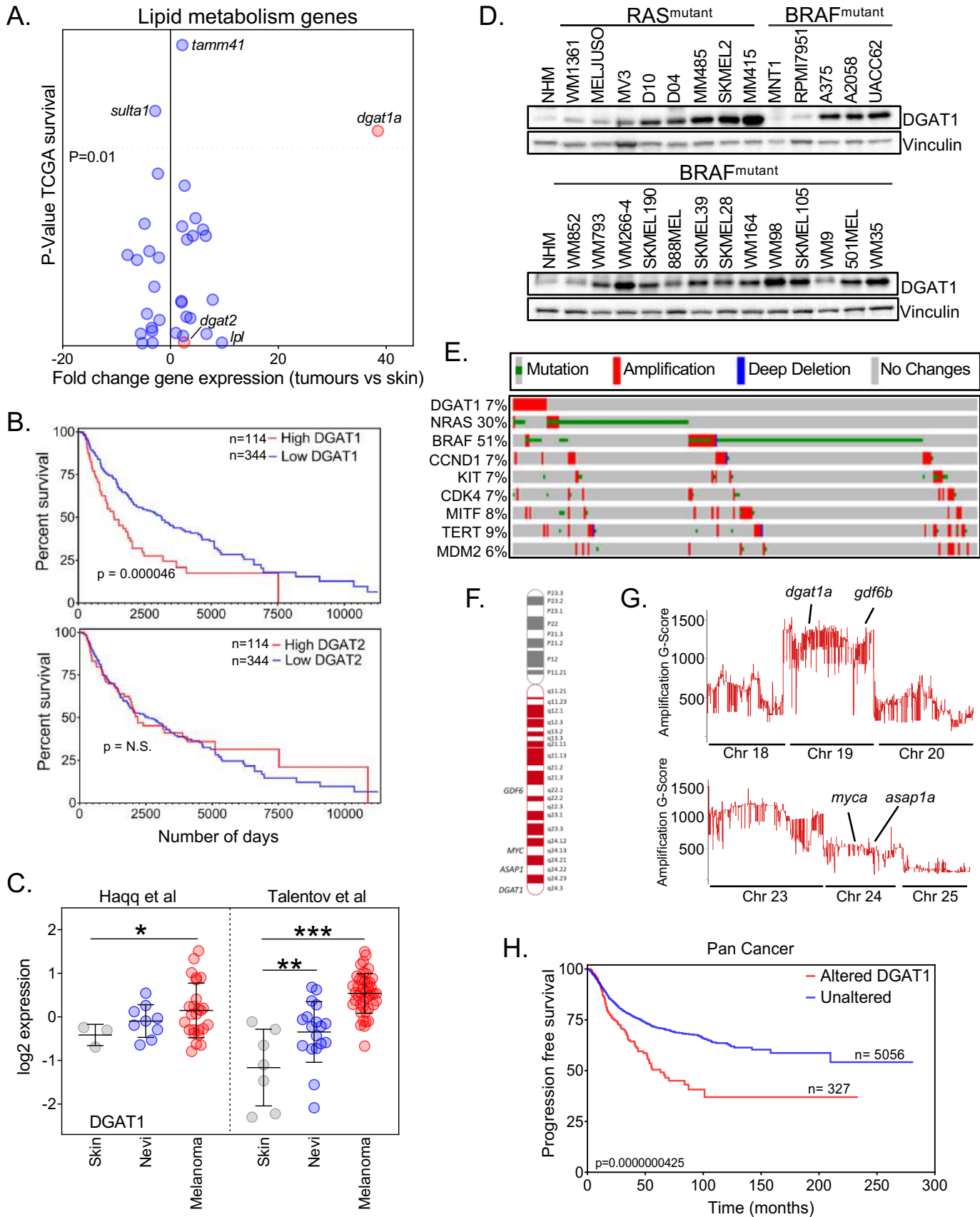
Figure 1 *DGAT1* amplification and up-regulation is associated with poor prognosis in melanoma

A. BRAF NRAS DGAT1
No Changes Mutation Amplification

B. $tp53^{M214K/M214k}; mitfa^{-/-}$

Melanoma incidence

Time to Tumour in Weeks

P=0.002

Tg(*mitfa:egfp*) — Tg(*mitfa:dgat1a*)

C. $tp53^{M214K/M214k}; mitfa^{-/-}; BRAF^{V600E}$

Melanoma incidence

Time to Tumour in Weeks

P=0.02

Tg(*mitfa:egfp*) — Tg(*mitfa:dgat1a*)

D. $tp53^{M214K/M214k}; mitfa^{-/-}; NRAS^{G12D}$

Melanoma incidence

Time to Tumour in Weeks

n.s.

P =0.0001

Tg(*mitfa:dgat2*)

Tg(*mitfa:egfp*) — Tg(*mitfa:dgat1a*)

E. Tg(*mitfa:egfp*)

Tg(*mitfa:dgat1a*)

F. -log10 (adjusted *P*)

log2 fold change

dgat1a

G. DGAT1 Expression

Patients

○ DGAT1 Low
○ DGAT1 High

Gene Sets

801 (48%)   92 (5.5%)   778 (46.5%)

Zebrafish *dgat1a* Over-expression   TGCA *DGAT1* High

H.

Translation
Eukaryotic Translation Elongation Homo sapiens
HALLMARK MTORC1 SIGNALING
HIF1A and PPARG regulation of glycolysis
cellular protein metabolic process
Metabolic Reprogramming in Cancer
CAMP UP.V1 UP
Focal Adhesion-PI3K-Akt-mTOR-signaling pathway
ATP metabolic process
HALLMARK ADIPOGENESIS
mTOR Signaling Activation by Fatty Acids and Glucose

-log P
1.4
2.9
4.4
5.9

Zebrafish *dgat1a* Over-expression
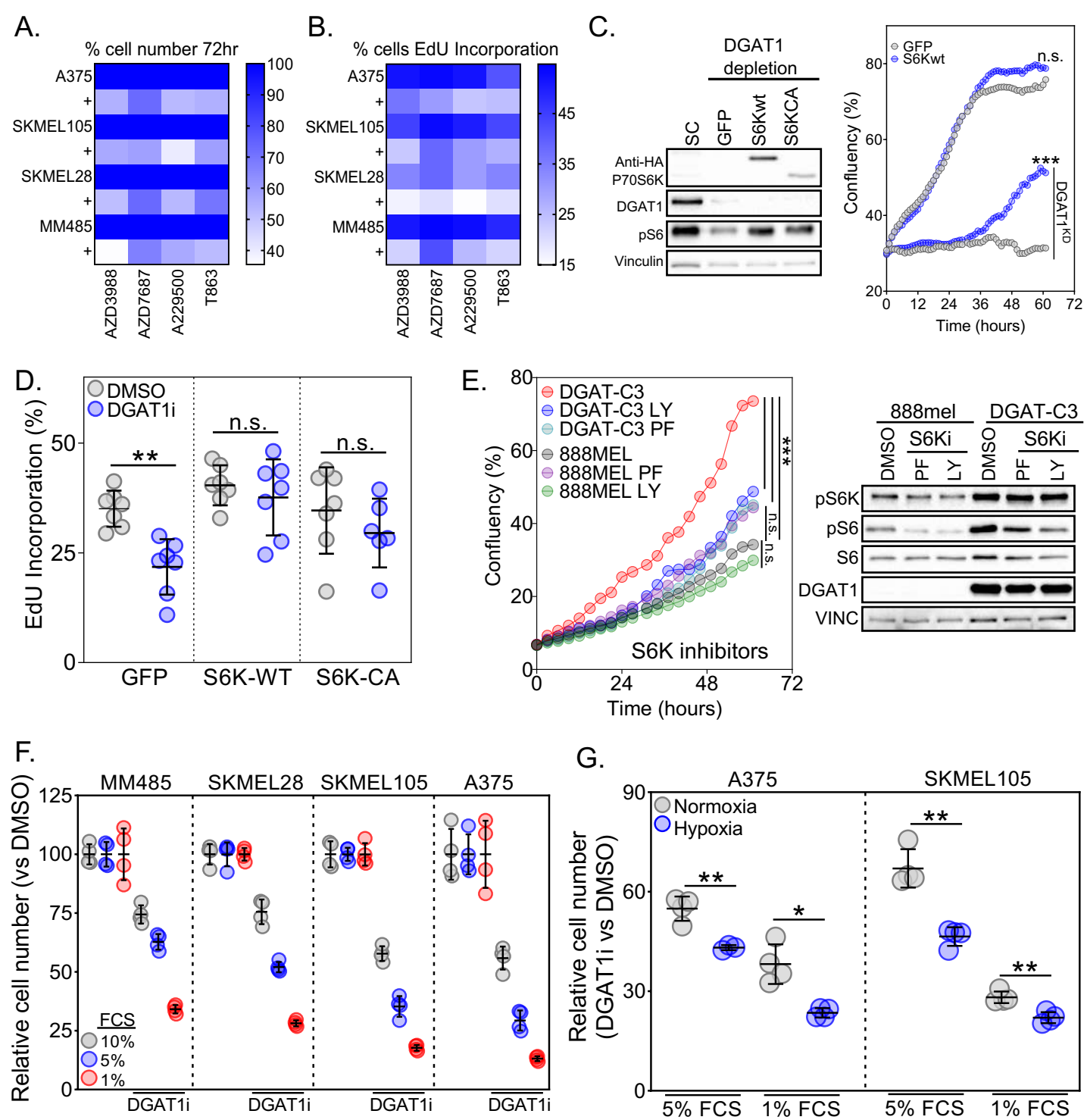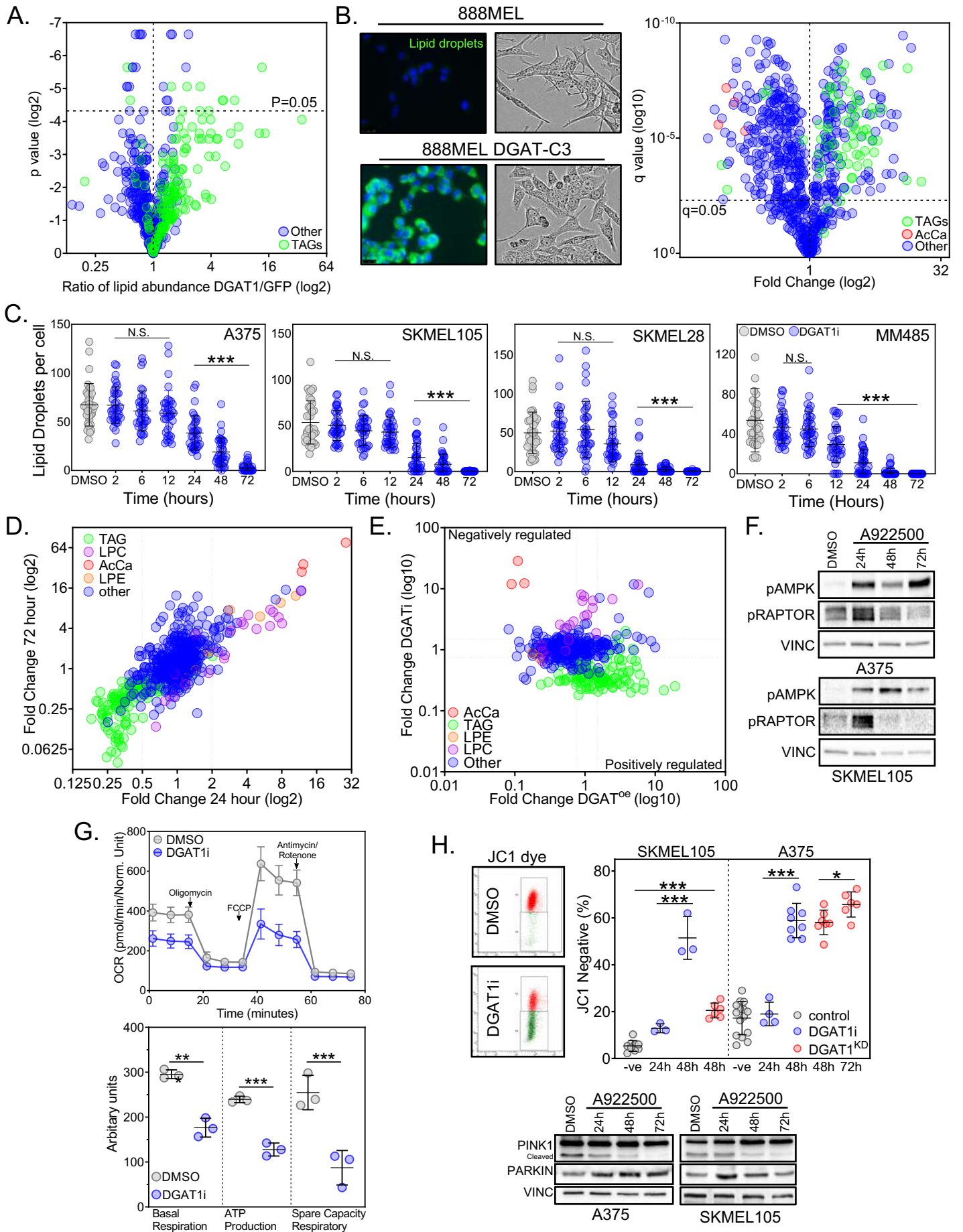
TGCA *DGAT1* High

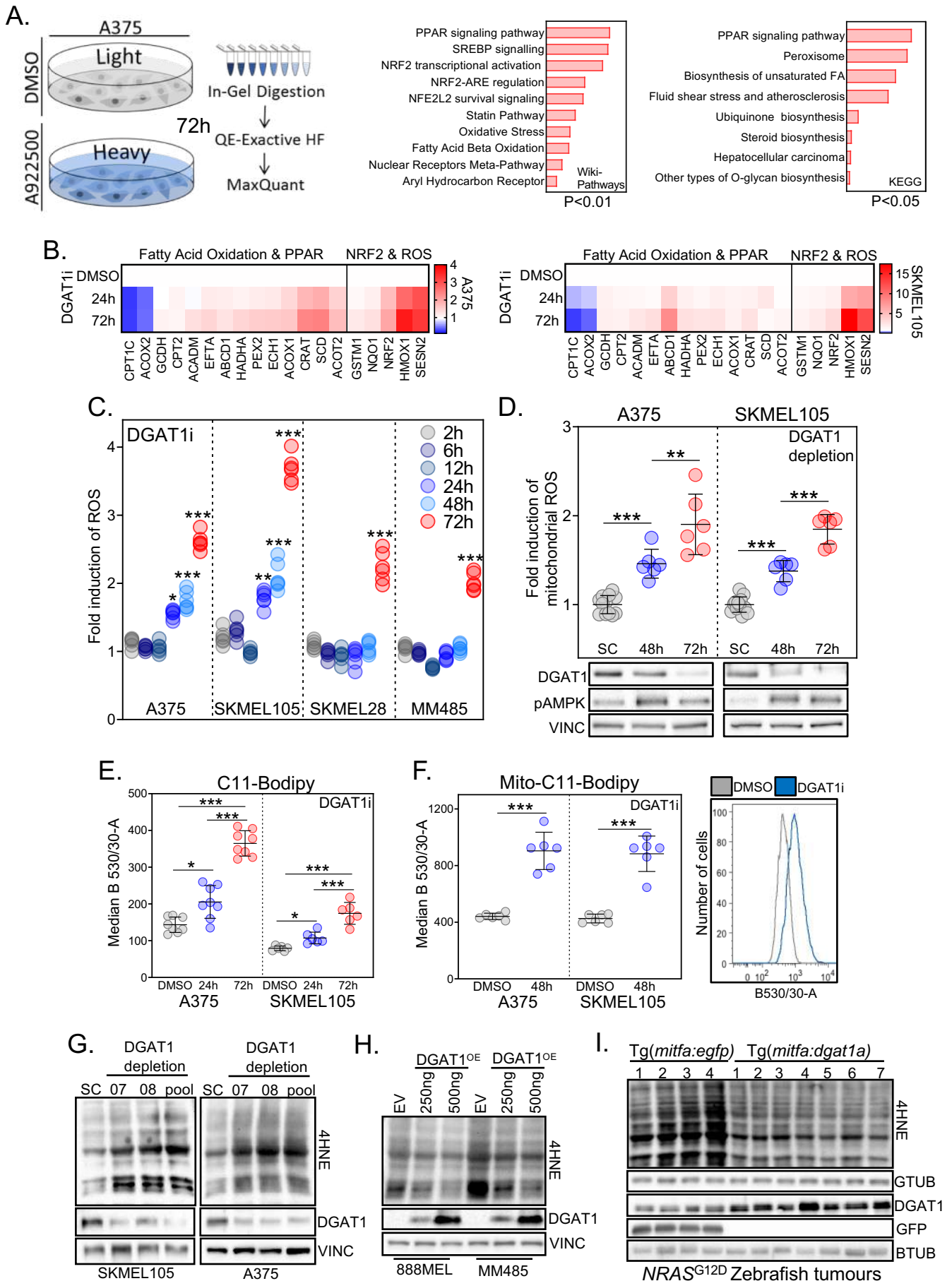**Figure 2 Dgat1 functions as an oncoprotein in zebrafish**

Figure 3 DGAT1 activity is required for maintenance of S6K signalling

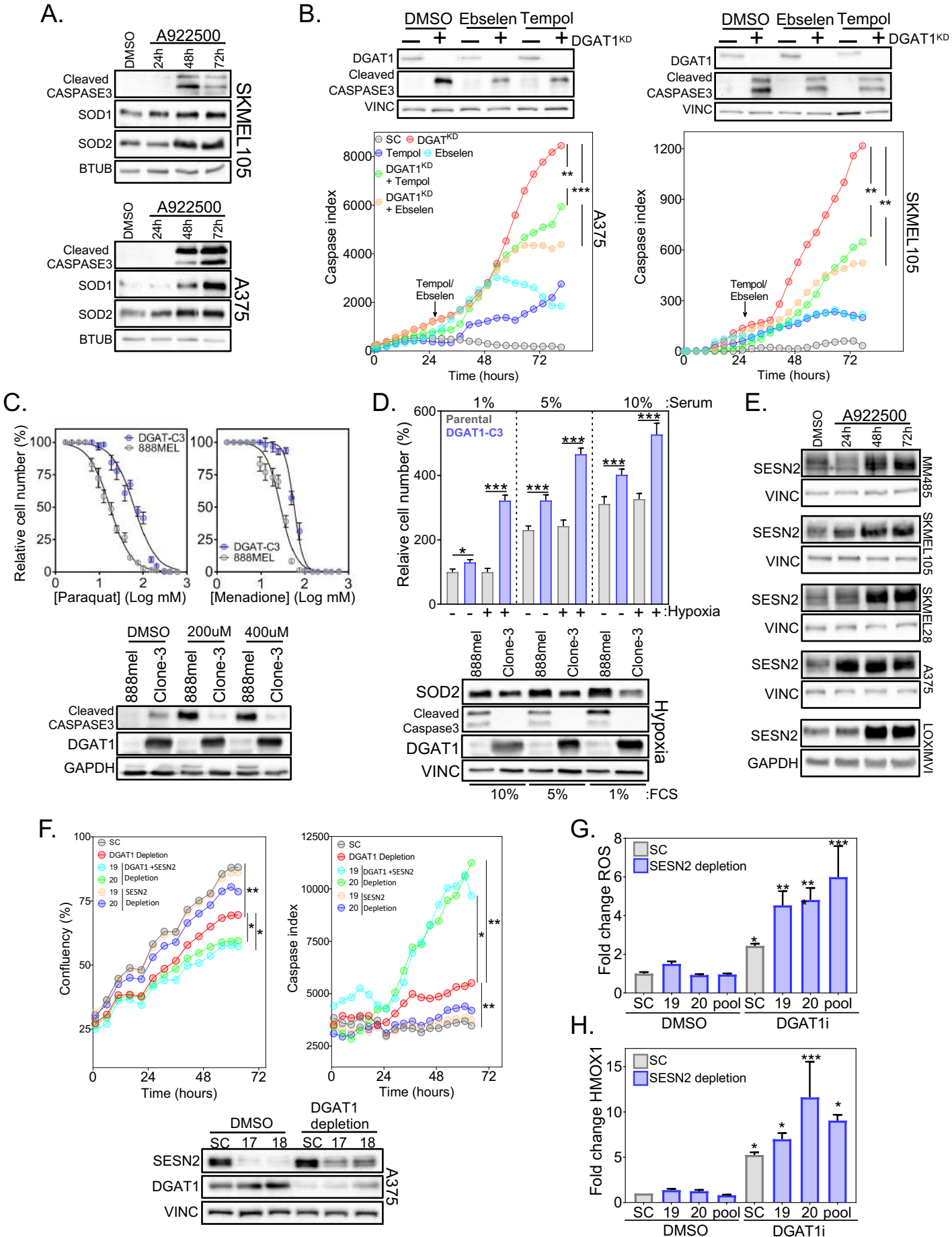**Figure 4 DGAT1 supports S6K dependent melanoma cell growth**

Figure 5 DGAT1-driven lipid droplets act as caretakers of mitochondrial health

Figure 6 DGAT1 suppression generates ROS leading to mitochondrial lipid peroxidation

Figure 7 DGAT1 suppression triggers ROS induced apoptosis that is ameliorated by SESN2